United States Department of Agriculture

Improved Models for Predicting the Modulus of Rupture of Lumber under Third Point Loading

Steve P. Verrill
Frank C. Owens
Rubin Shmulsky
Robert J. Ross

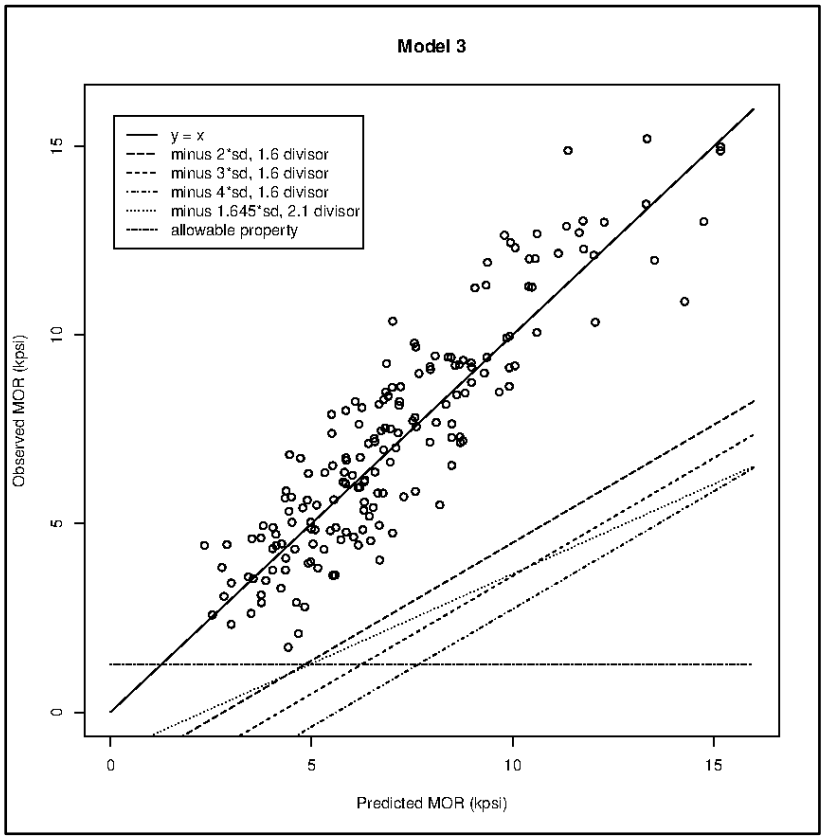

Forest Service | Forest Products Laboratory | Research Paper FPL–RP–712 | December 2021

Abstract

To properly evaluate the reliability of lumber structures, good models for the strength distributions of their components are needed. Modulus of rupture (MOR) distributions of structural lumber grades have often been modeled as two-parameter Weibulls. However, in a series of papers, Verrill and others have established that strength properties of visual and machine stress rated grades of lumber are not distributed as two-parameter Weibulls and that modeling them as two-parameter Weibulls can yield large over- or underestimates of probabilities of breakage. Instead, grades of lumber have "pseudo-truncated" distributions. Recent research also established that the appropriate MOR model can change significantly with location and time and that model differences have practical significance. Verrill and others concluded that "there may be significant efficiencies that can be obtained through the development of computer models that yield real-time in-line estimates of lumber properties based on measurements of stiffness, specific gravity, knot size and location, slope of grain, and other strength predictors." In this paper, we discuss models that predict the MOR of a piece of lumber from modulus of elasticity, specific gravity, slope of grain, and knot data.

Keywords: modulus of rupture, modulus of elasticity, specific gravity, slope of grain, knots, Weibull distribution, pseudo-truncated distributions, strength prediction models, lumber strength models

December 2021

Verrill, Steve P.; Owens, Frank C.; Shmulsky, Rubin; Ross, Robert J. 2021. Improved models for predicting the modulus of rupture of lumber under third point loading. Research Paper FPL-RP-712. Madison, WI: U.S. Department of Agriculture, Forest Service, Forest Products Laboratory. 38 p.

A limited number of free copies of this publication are available to the public from the Forest Products Laboratory, One Gifford Pinchot Drive, Madison, WI 53726-2398. This publication is also available online at www.fpl.fs.fed.us. Laboratory publications are sent to hundreds of libraries in the United States and elsewhere.

The Forest Products Laboratory is maintained in cooperation with the University of Wisconsin.

The use of trade or firm names in this publication is for reader information and does not imply endorsement by the United States Department of Agriculture (USDA) of any product or service.

Contents

Improved Models for Predicting the Modulus of Rupture of Lumber under Third Point Loading

Steve P. Verrill, Mathematical Statistician
USDA Forest Service, Forest Products Laboratory, Madison, WI

Frank C. Owens, Assistant Professor
Department of Sustainable Bioproducts, Mississippi State University, MS

Rubin Shmulsky, Professor and Department Head
Department of Sustainable Bioproducts, Mississippi State University, MS

Robert J. Ross, Supervisory Research General Engineer
USDA Forest Service, Forest Products Laboratory, Madison, WI

1 Introduction

To properly evaluate the reliability of lumber structures, it is necessary to have good models for the strength distributions of their components. In the past, the modulus of rupture distribution of structural lumber has often been modeled as a two-parameter Weibull. Verrill et al. (2012, 2013, 2014, 2015, 2019, 2020a) established theoretically and empirically that the strength properties of visual and MSR grades of lumber are not distributed as two-parameter Weibulls, and that modeling them as two-parameter Weibulls can yield large over- or underestimates of probabilities of breakage. This led Verrill et al. (2017, 2018, 2020b), Owens et al. (2018, 2019, 2020), and Anderson et al. (2021) to investigate alternative models for strength distributions of lumber. However, Verrill et al. (2020b) demonstrated that even if we have adequate models for the *general parametric forms* of distributions (e.g., pseudo-truncated Weibull or pseudo-truncated mixed normal or ...), the *specific* strength distributions (due to specific parameter values) can vary significantly (from a practical as well as a theoretical viewpoint) with mill and time. They argued that this variability suggests that "there may be significant efficiencies that can be obtained through the development of computer models that yield real-time in-line estimates of lumber properties based on measurements of stiffness, specific gravity, knot size and location, slope of grain, and other strength predictors." In this paper we discuss models that predict the modulus of rupture (MOR) of a piece of lumber from modulus of elasticity (MOE), specific gravity (SG), slope of grain (SOG), and knot data. We have fit these models to the summer data discussed in Owens et al. (2018, 2019, 2020). In a later paper we plan to investigate whether predictors associated with rings per inch, percentage of latewood, distance to the pith, and location on a flatsawn to quartersawn spectrum improve the fit.

2 Recent Literature

A good deal of recent research activity has been aimed at producing better estimates of the strengths of individual pieces of lumber. This work has been motivated by a recognition that advances in computing and in high-speed X-ray scanning, laser scanning, and computer tomography devices should permit us to develop, fit, and deploy models that permit much more efficient use of our timber resources. See, for example, the "Motivation and Purpose of This Project" section in Hanhijärvi and Ranta-Maunus (2008) or the "State of the Art" section in Lukacevic et al. (2015).

In Table 1 we identify a few of these studies and list some of their features. The most important feature, s, the root mean squared error, appears in the last column of the table. Unfortunately, s is sometimes missing which makes it hard to compare the effectiveness of all the approaches (see Section 3). Also, we suspect that differences in species, board sizes, board grades, and moisture content variability and a failure to test a fit on a *new* set of data (or, alternatively, to perform a cross-validation) may make direct comparisons difficult.

Having said this, we do wish to comment on a few of these recent papers. In some cases, these remarks further highlight the difficulties in making direct comparisons. In others, we are interested in highlighting similarities in or differences between their work and our own.

Wright et al. (2019) make use of k-means clustering to automatically identify and measure knots in images of board faces. Their best model is a linear model with specific gravity, acoustic velocity, and knot area fraction as predictors of MOR. They obtain a root mean squared error of 7.2 megapascals (MPa). The root mean squared errors (RMSE) of our models, for example, are approximately 9.4 MPa (see the s values in Tables 3–7). Their model could be superior to ours. However, there are other possible explanations. First, one of their predictors is knot area fraction, the fraction of area covered by knots in a particular span of a board. However, their particular span of a board is chosen to minimize the root mean squared error (see their figure 3) for their particular data set. The resulting procedure (based on the span fraction that minimized root mean squared error for their data set) may not yield equally good results for new data sets. Second, when they fit MOR to specific gravity (as the sole predictor), they obtain a RMSE of 9.2 MPa for their data set. (See their figure 6.) However, when we fit MOR to specific gravity (as the sole predictor), we obtain a RMSE of 15.8. Thus, there may be a basic difference in the natural variability of our data sets. Their lumber is apparently all loblolly pine, sawn at a single mill. Our lumber may include other southern yellow pine species and comes from 3 mills. Their lumber is either No. 1 or No. 2 visual grade, whereas our lumber is mill run lumber. Finally, their lumber is 2×6 or 2×8 lumber, whereas ours is 2×4 lumber. Thus, it is possible that our results are not directly comparable to theirs.

Schajer's work (2001) is X-ray based, but his nonlinear model is similar in some ways to our models. His knot factor is a minimum over vertical lines across a face (lines perpendicular to a lengthwise edge), as are our knot factors for Models 4 and 5. (However, because Schajer works with X-rays, he obtains information on a full cross-section, not just visual information based on vertical lines on the front and back faces.) Also, his "wood structural factor" involves terms for three separate lengthwise bands — a compression edge band, a central band, and a tension edge band, whereas our model considers four lengthwise bands — compression edge, compression near center, tension near center, and tension edge.

And just as we obtained Model 2 and Model 3 results (see Section 5) that suggest that knots in the compression near center region might *increase* bending strength (see the negative band 2 powers in our Tables 4 and 5), Schajer's model (2001) predicts that knots in his central region might increase bending strength (see the negative w_2 values in the group 5 section of his table 6).

We have discussed this result with Professor Schajer. He feels that the result is physically implausible and likely an artifact of the unit sum constraint of the weights used in his model. With this in mind, he argues that an alternative interpretation of the negative center strength reduction coefficient in his model is that a defect there is much less damaging to bending strength than defects in the outer regions. The center area looks attractive only relative to its very adverse neighbors.

We would argue that it is possible that the slightly positive effect of a knot in the compression midline region could be real. This effect is in line with, for example, the results in Cao et al. (2018).

The facts that 1) the band 4 (tension edge) powers in our Tables 4 – 6 exceed the corresponding band 1 (compression edge) powers, and 2) our band 4 strength factor lies below our band 1 strength factor in Table 7 are in accord with Schajer's (2001) w_3 value exceeding his w_1 value in the 3-unsymmetric line in the group 5 section of his table 6. These results suggest that tension edge knots lead to greater strength reductions than do comparably sized compression edge knots (and the results quantify this difference).

Olsson et al. (2013) predicted MOR from local fiber orientation and the resonance frequency of the first longitudinal mode of vibration. They took into account the manner in which load varied outside of the central 1/3 of the board. We have also taken this into account in our calculations. See the discussion of parameters β_9 and β_{10} in Section 5.2, and the discussion of the denom_j values in Sections 5.4 and 5.5.

Olsson et al. (2017) expands Olsson et al. (2013) by fitting a new data set composed of a total of 900 pieces of lumber of 10 different sizes gathered from 9 separate sites. For this data set they report a prediction error of 6.3 MPa. This value is well-below other values reported in the literature. (See Table 1.) This might be expected given their use of new technology and careful theoretical analyses. We do note, however, as mentioned above, that differences in species, board sizes, board grades, and moisture content variability and a failure to test a fit on a *new* set of data (or, alternatively, to perform a cross-validation) might make direct comparisons difficult. We also note that we do see an opportunity for Olsson et al. and other authors to improve their models by adopting a feature of our model (and of Schajer's model) that distinguishes between tension and compression edges. See Section 10.2 for details. (We recognize that, currently, one cannot be certain of the orientation in which a carpenter or contractor will install a given joist, rafter, or other bending member at a job site. The ability to identify and mark an optimal tension edge may prove to be practically useful only for manufactured housing.)

The system described in Olsson et al. (2017) has been approved for commercial use in Europe.

Lukacevic et al. (2015) is an interesting paper. It includes an extensive and useful literature review, introduces a number of proposed strength predictors ("indicating properties" or IPs), considers a large number of models, and obtains some high R^2's (as high as .89) and, apparently, small mean squared errors. However, for bending strength, it contains only 43 data points (29 for tensile strength) while considering 23 predictors. It is true that the authors' best bending model includes only 7 or 8 parameters (8 if their linear regression included a constant term) and they made use of Mallow's C_p statistic. However, the C_p statistic does not necessarily protect a scientist from overparameterizing a model. In an effort to improve accuracy, scientists sometimes fail to wield Occam's razor and end up with overly complex models (too many predictors) that predict the data used in the fitting process quite well, but perform relatively poorly on new data. As discussed in Section 7 ("Avoiding error underestimation"), the best protection against an overestimate of a model's predictive ability is the use of fit and test data sets (or, as an alternative, cross-validation procedures). We note that none of our references makes use of such a technique and thus, to some extent, they all probably tend to overestimate R^2's and to underestimate s values.

Lukacevic et al. (2015) also perform both "manual" and "automatic" "reconstructions" that yield knot data that are used to generate their predictors. Manual methods could not be used to yield real-time in-line strength predictions. For boards tested in tension, the automatic methods yielded R^2 values that are significantly lower than the R^2 values associated with the manual methods. For boards tested in bending, the authors did not compare automatic and manual methods.

Lukacevic et al. (2015) also suggest via their "weighting functions" that knots on the compression side of a board undergoing edgewise bending have little or no effect on a board's modulus of rupture (MOR) and have a monotically increasing effect (linear or quadratic) as the knots become closer to the tension edge. Our results and those of Schajer (2001) (see the discusssion of Schajer's paper above) do not support this claim. (Also see the discussion of compression edge, center, and tension edge knots in Kretschmann (2010).) Our "band" powers in Tables 4-6 and strength factors in Table 7 suggest that knots in the compression edge band certainly have a greater effect on board strength than do knots in the near-midline compression band and may have a greater effect on board strength than knots in the near-midline tension band. Schajer's work (see the "3-profile density measurements" section of Schajer, 2001) suggests that tension edge knots have a greater effect than compression edge knots, but that compression edge knots have a greater effect than midline knots. We do not have an explanation for the discrepancy between our results (and those of Schajer) and the results of Lukacevic et al. (2015).

3 Aside: R^2 versus s

It is a common (although not universal) practice among scientists and engineers to take R^2, the correlation squared between observed and predicted values, as a measure of the "quality" or "predictive ability" of a linear regression.

However, there is a problem with this approach. For a linear regression with a constant term,

$$R^2 = 1 - \sum_{i=1}^{n}(y_i - \hat{y}_i)^2 / \sum_{i=1}^{n}(y_i - \bar{y})^2 \tag{1}$$

where y_i is the ith observed value, $\hat{y}_i$ is the ith predicted value, $\bar{y}$ is the mean of the y_i values, and R is the correlation between the y_i's and $\hat{y}_i$'s. For a model with p parameters,

$$s^2 \equiv \sum_{i=1}^{n}(y_i - \hat{y}_i)^2/(n-p) \tag{2}$$

is an estimate of the variability of observed values about predicted values. The smaller a model's s^2 is, the better the model's predictions will be.

We want to develop strength prediction models with low prediction errors, that is with low s^2 values. From Equations (1) and (2) we see that

$$R^2 = 1 - s^2 / \left(\sum_{i=1}^{n}(y_i - \bar{y})^2/(n-p) \right) \tag{3}$$

From Equation (3) we see that we can have high R^2 values if *either* s^2 is low (which is ultimately what we want) or $\sum_{i=1}^{n}(y_i - \bar{y})^2/(n-p)$ is high. s^2 is telling us how good our predictions are, but $\sum_{i=1}^{n}(y_i - \bar{y})^2/(n-p)$ is, essentially, just telling us how spread out our predictors are. This sensitivity of R^2 values to the range of predictor values is

the reason that R^2 should not, in general, be used to compare the qualities of fits in a range of studies. (*Roughly* speaking, R^2 values can be used to compare fits when the "x" [predictor] ranges in the studies are the same.)

For example, we found that our R^2 values exceeded those found in all but one of the studies that we reference. However, we are working with "mill run" data. That is, the visual grades of our lumber specimens varied in quality from below "No. 3" to "Select Structural." This will tend to maximize $\sum_{i=1}^{n}(y_i - \bar{y})^2$ values and thus maximize R^2 values.

Unfortunately, some of our references report only R^2 values. Thus, in Table 1b in the absence of s^2 values we report R^2 values (as well as s^2 values when available) even though the R^2 values can be misleading.

We also note that our models are "nonlinear in the parameters" (see Section 5). Equation (1) need not hold if we are working with a nonlinear regression model, or with a linear model that does not include a constant term. However, for linear models that do contain a constant term, the R^2 value in (1) also equals the correlation squared between the observed and predicted values — that is,

$$R^2 = \left(\frac{\sum_{i=1}^{n}(y_i - \bar{y})(\hat{y}_i - \bar{\hat{y}})}{\sqrt{\sum_{i=1}^{n}(y_i - \bar{y})^2 \sum_{i=1}^{n}(\hat{y}_i - \bar{\hat{y}})^2}} \right)^2 \tag{4}$$

where y_i is the ith observed value, $\hat{y}_i$ is the ith predicted value, $\bar{y}$ is the mean of the y_i values, and $\bar{\hat{y}}$ is the mean of the predicted values. We can use definition (4) to calculate and compare R^2 values for both linear and nonlinear models. The R^2 values that we report in Table 1b are calculated via definition (4).

4 Data

The data collection process is described in detail in Owens et al. (2018, 2019, 2020). It yielded eight samples (four mills at two times) of southern pine (*Pinus* spp.) 2×4 lumber, each containing approximately 200 pieces.

The techniques that were used to estimate MOR and stiffness are described in Owens et al. (2018, 2019, 2020).

Specific gravity was measured by cutting a test piece from the end of each specimen immediately after rupture in the static bending machine. The test piece was cut in full cross section approximately one inch from the end of the specimen. That piece was immediately weighed in grams, measured volumetrically in cubic millimeters, and then oven dried to 0% moisture content. The density in kilograms per cubic meter was calculated by dividing the oven dry mass by the volume at the time of testing and subsequently converted to specific gravity by dividing by the density of water (1000 kg per cubic meter).

Slope of grain was measured with the Metriguard Model 511 Grain Angle Meter. The meter estimates slope of grain for a piece of lumber by calculating the angle between the maximum permittivity direction (projected onto the face of the piece of lumber) and the lengthwise midline of the piece of lumber. It provides readings from 0 to a maximum of 23.9 degrees. (Angles greater than 23.9 degrees are reported as 23.9 degrees.) The meter was positioned on a randomly chosen broad face of each specimen and manually slid along the span between the load heads (plus 2.5 inches at each end of the span). The operator read and manually recorded the maximum angle reading.

Knot locations and sizes were estimated from photographic (pre-test) images of both faces of the boards. To obtain this information we used a Java image analysis program written by one of the authors. (The program can be obtained at `http://www1.fpl.fs.fed.us/knots_2x4.html`.) The program permits a user to calibrate a board image, to fit an ellipse to each observed knot (based on eight mouse clicks per knot), and to determine (based on a 200 by 1800 grid) 1) the approximate area of intersection of each knot with each of the 4x6 rectangular regions into which we divide a face of the board (see Table 2 and Section 5) and 2) the fractions of the 1800 vertical grid lines on a face that lie in a knot (see Section 5). The Java program also permits a user to study magnified images of arbitrary sections of the board and to make the eight clicks that are used to fit an ellipse to a knot on a magnified image of the knot and its immediate surroundings. It also permits a user to record comments about each board as it is analyzed. The program is described in greater detail in Verrill et al. (2021).

The MOE values used in our analyses are in millions of pounds per square inch. The MOR values are in thousands of pounds per square inch (kpsi). The SOG values are in degrees. The knot values enter our equations as dimensionless area or length fractions (see Section 5).

Our current work covers only the "summer" data from three of the Owens et al. (2018, 2019, 2020) mills. Summer images were not available from one of the mills. Thus, only 600 pieces of lumber were considered in this study. Before our analysis we removed five pieces of lumber from consideration. One broke before being tested. Two were rejected

because of extreme crook. Two were rejected because they contained large holes that extended from one face to the other. In the course of our analysis we also identified 10 visual outliers. For five of these outliers we could find no justification for rejecting them and we retained them in our final data set. The other five outliers were removed from the data set because one had 6 large "punches" in a line near or on the tension edge, a second had severe cracks, and the remaining three displayed clear "machine damage" (saw/scrape/grip damage).

An early reviewer of this paper questioned whether it was appropriate to treat the three "machine damage" specimens as rejectable outliers. The reviewer suggested that "normal" below No. 3 visual grade specimens can often display "machine damage" and yet be used in structures. In response to this reviewer's observation, for each of Models 2-5 (discussed in Section 5), we performed four fits: a fit of 590 observations that did not include the five outliers, a fit of 593 observations that did include the three "machine damage" outliers, a fit of the 469 No. 3 and above boards (which included one of the three "machine damage" outliers), and a fit of the 327 No. 2 and above boards (which included none of the three "machine damage" outliers). The root mean squared errors associated with these fits are provided in Tables 4–7.

We would argue that the fits suggest that it is reasonable to work with the 590 observation data set. We do so in the remainder of this paper.

5 Models

For the most part, we used nonlinear regression models rather than linear regression models. Nonlinear regression fitting routines are readily available in statistical packages and can more accurately model physical relations that are inherently nonlinear. Here "nonlinear" has a technical meaning that differs from "not a straight line." For example, $y = \beta_0 + \beta_1 \times x + \beta_2 \times x^2 + \epsilon$ (where ϵ is a random error term) is a "linear model" even though its plot is a curved line. If a model can be written as

$$y = \beta_1 \times g_1(\mathbf{x}) + \ldots + \beta_p \times g_p(\mathbf{x}) + \epsilon$$

where the β_i's are the parameters and the g_i's are solely functions of the predictor variables (e.g., stiffness, specific gravity, ...) and do not involve the β_i's, then it is "linear in the parameters" and can be fit via a linear regression. If, however, the model has the form $y = f(\mathbf{x}; \boldsymbol{\beta}) + \epsilon$ where $\mathbf{x}$ is the predictor vector and $\boldsymbol{\beta}$ is the parameter vector, and if, for some i, $\partial f(\mathbf{x}; \boldsymbol{\beta})/\partial \beta_i$ contains at least one of the β parameters, then the model is nonlinear in its parameters and nonlinear regression routines must be used. For example, the model $y = a \times e^{\beta x} + \epsilon$ would need to be handled via a nonlinear regression.

5.1 Model 1: Non-Hankinson SOG factor. No knot factor.

$$\text{MOR} = \beta_1 \times \text{MOE}^{\beta_2} \times \text{SG}^{\beta_3} \times (90 - |\text{SOG}|)^{\beta_4} \tag{5}$$

5.2 Model 2: Non-Hankinson SOG factor. Knot factor based on knot areas on wide faces ("non-KAR" where "KAR" stands for "Knot Area Ratio").

$$\text{MOR} = \beta_1 \times \text{MOE}^{\beta_2} \times \text{SG}^{\beta_3} \times (90 - |\text{SOG}|)^{\beta_4} \times (\text{knot factor})_{\text{A}} \tag{6}$$

where $(\text{knot factor})_{\text{A}}$ equals the *minimum* of the 6 knot factors associated with the 6 columns in Table 2 where the column 1 factor equals

$$(1 - p_{11})^{\beta_5} \times (1 - p_{21})^{\beta_6} \times (1 - p_{31})^{\beta_7} \times (1 - p_{41})^{\beta_8}/\beta_9$$

the column 2 factor equals

$$(1 - p_{12})^{\beta_5} \times (1 - p_{22})^{\beta_6} \times (1 - p_{32})^{\beta_7} \times (1 - p_{42})^{\beta_8}/\beta_{10}$$

the column 3 factor equals

$$(1 - p_{13})^{\beta_5} \times (1 - p_{23})^{\beta_6} \times (1 - p_{33})^{\beta_7} \times (1 - p_{43})^{\beta_8}/1$$

the column 4 factor equals

$$(1 - p_{14})^{\beta_5} \times (1 - p_{24})^{\beta_6} \times (1 - p_{34})^{\beta_7} \times (1 - p_{44})^{\beta_8}/1$$

the column 5 factor equals

$$(1-p_{15})^{\beta_5} \times (1-p_{25})^{\beta_6} \times (1-p_{35})^{\beta_7} \times (1-p_{45})^{\beta_8}/\beta_{10}$$

the column 6 factor equals

$$(1-p_{16})^{\beta_5} \times (1-p_{26})^{\beta_6} \times (1-p_{36})^{\beta_7} \times (1-p_{46})^{\beta_8}/\beta_9$$

and the p_{ij} values are the knot area fractions (averaged across both faces of a board) in the 24 board regions illustrated in Table 2.

At first glance, the knot factor appears quite complex. In fact, however, the factor simply attempts to reflect four physical facts.

First, larger knots are expected to yield larger reductions in strength. This is reflected in the $1-p$ factors, which will be smaller for regions that contain more knot area.

Second, there is a compression edge and a tension edge. Under third point loading, engineers expect that the effects of knots will be largest at the edges and smallest in the center of the board. This action occurs because bending strength is related to the square of section depth. Further, the effects of sound (solid) knots are expected to be lower under compression than under tension. Unsound knots, however, are considered as holes and are equally detrimental in either case. The powers β_5, β_6, β_7, β_8 permit the effects of knots to differ among 4 regions: the compression band nearest to the compression edge, the compression band nearest to the center of the board, the tension band nearest to the center of the board, and the tension band nearest to the tension edge. To some degree this is an oversimplification of the bending stress within the depth of a beam's section, but for the intents and purposes herein the approximation is prudent.

Third, under (one-)third point loading (that is, four point bending with equal loads applied at the one-third and two-thirds points of the span), the stress level is constant along the length of the beam between the two load heads, and decreases outside of the load heads as one approaches the support or reaction points. Given our model, we would expect this change to be reflected by the relation $1 > \beta_{10} > \beta_9$.

Fourth, engineers expect that failure will occur in the region in which a "weakest link" in relation to load occurs. Under third point loading engineers often expect crack failure to initiate at an edge and to propagate roughly "across a board" through its cross-section. That expectation assumes that the strength is relatively homogeneous throughout the volume of the member. Thus, by taking strength to be associated with the minimum of the 6 products listed above, we are assuming that they reflect the "strengths" of 6 "vertical" pathways across the board *taking into account the distinct loads that are seen in the pathways* (hence the divisors β_9, β_{10}, and 1).

We recognize that this ad hoc model can be improved by careful engineering analysis. We also understand that third point loading does not necessarily reflect actual loads on structural members in floors, walls, and trusses. It does however permit repeatable analysis and investigation among specimens, samples, and populations over time. Here, we are focused on closing the gap between predicted and observed strengths given current testing methods. We believe that for *maximum* efficiency, strength models would need to incorporate expected load patterns in various structural members (floors, walls, trusses, ...) and boards would need to be marked and separated on the basis of intended end use. In the stick-built world, such expectations are likely impractical. But in the case of factory built housing, where quality control can be better managed, this level of detail might be possible.

5.3 Model 3: Hankinson SOG factor. Knot factor based on knot areas on wide faces ("non-KAR").

$$\mathrm{MOR} = \beta_1 \times \mathrm{MOE}^{\beta_2} \times \mathrm{SG}^{\beta_3} \times R(\theta) \times (\text{knot factor})_{\mathrm{A}} \tag{7}$$

where θ is the absolute value of the slope of grain and $R(\theta)$ is the reduction factor given by Hankinson's formula:

$$R(\theta) = (Q/P) \,/\, (\sin^{\alpha}(\theta) + (Q/P) \times \cos^{\alpha}(\theta)) \tag{8}$$

where P is the strength parallel to grain, Q is the strength perpendicular to grain, and α is an empirical power. (This adds two parameters to the model, Q/P and α, and drops one — Model 2's β_4.) The knot factor in Model 3 is the same as the knot factor in Model 2.

5.4 Model 4: Hankinson SOG factor. Knot factor based on vertical "heights" on wide faces ("KAR" approach 1).

$$\text{MOR} = \beta_1 \times \text{MOE}^{\beta_2} \times \text{SG}^{\beta_3} \times R(\theta) \times (\text{knot factor})_{\text{B}} \tag{9}$$

where $R(\theta)$ is given by Equation (8). The knot factor in Model 4 ($(\text{knot factor})_{\text{B}}$) differs from that in Models 2 and 3. Rather than being based on the fraction of *knot area in a region*, it is based on the fraction of *knot height in a vertical line across a board face* (in line with KAR concepts). In particular the knot factor is the minimum over 1800 vertical lines (from left support to right support) of the product

$$\begin{aligned}&(1 - f_{1j} + a \times f_{1j})^{\beta_6} \\ &\times(1 - f_{2j} + a \times f_{2j})^{\beta_7} \\ &\times(1 - f_{3j} + a \times f_{3j})^{\beta_8} \\ &\times(1 - f_{4j} + a \times f_{4j})^{\beta_9}/\text{denom}_j\end{aligned} \tag{10}$$

where $j \in \{1, \ldots, 1800\}$, $\text{denom}_j = j/601$ for $j \in \{1, \ldots, 600\}$, $\text{denom}_j = 1$ for $j \in \{601, \ldots, 1200\}$, $\text{denom}_j = (1801 - j)/601$ for $j \in \{1201, \ldots, 1800\}$, f_{1j} is the knot fraction (averaged across both board faces) in the upper fourth (compression region nearest to the compression edge) of the jth of the 1800 vertical lines across a board face, f_{2j} is the knot fraction (averaged across both board faces) in the second fourth (compression region nearest to the middle of the face) of the jth of the 1800 vertical lines, f_{3j} is the knot fraction (averaged across both board faces) in the third fourth (tension region nearest to the middle of the face) of the jth of the 1800 vertical lines, and f_{4j} is the knot fraction (averaged across both board faces) in the bottom fourth (tension region nearest to the tension edge) of the jth of the 1800 vertical lines, a (corresponding to parameter β_{10} in the model) provides for a reduction of strength over a knot, and β_6, β_7, β_8, and β_9 permit this reduction of strength over a knot to have greater or lesser effect depending on whether the knot is in the compression half or the tension half, and how close the knot material is to the nearest edge. The varying denom_j values permit us to account for the varying loads under (one-)third point loading.

5.5 Model 5: Hankinson SOG factor. Knot factor based on vertical "heights" on wide faces ("KAR" approach 2).

$$\text{MOR} = \beta_1 \times \text{MOE}^{\beta_2} \times \text{SG}^{\beta_3} \times R(\theta) \times (\text{knot factor})_{\text{C}} \tag{11}$$

where $R(\theta)$ is given by Equation (8). The knot factor in Model 5 $(\text{knot factor})_{\text{C}}$ is similar to the knot factor in Model 4. However, rather than having a constant a account for a strength reduction associated with a knot and β_6 – β_9 to account for four load regions (2 compression and 2 tension), we provide for regional differences by replacing a with β_6 – β_9 depending on the region. Both Models 4 and 5 are intuitively reasonable ad hoc models. We explored both models.

In Model 5 the knot factor is the minimum over 1800 vertical lines in a face (from left support to right support) of the product

$$\begin{aligned}&(1 - f_{1j} + \beta_6 \times f_{1j})^{\beta_{10}} \\ &\times(1 - f_{2j} + \beta_7 \times f_{2j})^{\beta_{10}} \\ &\times(1 - f_{3j} + \beta_8 \times f_{3j})^{\beta_{10}} \\ &\times(1 - f_{4j} + \beta_9 \times f_{4j})^{\beta_{10}}/\text{denom}_j\end{aligned} \tag{12}$$

where $j \in \{1, \ldots, 1800\}$, $\text{denom}_j = j/601$ for $j \in \{1, \ldots, 600\}$, $\text{denom}_j = 1$ for $j \in \{601, \ldots, 1200\}$, $\text{denom}_j = (1801 - j)/601$ for $j \in \{1201, \ldots, 1800\}$, f_{1j} is the knot fraction in the upper fourth (compression region nearest to the compression edge) of the jth of the 1800 vertical lines, f_{2j} is the knot fraction in the second fourth (compression region nearest to the middle of the face) of the jth of the 1800 vertical lines, f_{3j} is the knot fraction in the third fourth (tension region nearest to the middle of the face) of the jth of the 1800 vertical lines, and f_{4j} is the knot fraction in the bottom fourth (tension region nearest to the tension edge) of the jth of the 1800 vertical lines, and parameters β_6 – β_9 provide for a reduction of strength over a knot that depends on the lengthwise band. The varying denom_j values permit us to account for the varying loads under (one-)third point loading.

6 Fitting the Models

6.1 Model 1

Estimates of β_1, β_2, β_3, and β_4 in Model 1 were obtained by taking the log of both sides of Equation (5), and performing a linear regression on the model

$$\log(\text{MOR}) = \log(\beta_1) + \beta_2 \times \log(\text{MOE}) + \beta_3 \times \log(\text{SG}) + \beta_4 \times \log(90 - |\text{SOG}|) \tag{13}$$

The regression fit was performed via the lm method of the R statistical environment (R Core Team, 2018).

Estimates of the parameters of Model 1 are provided in Table 3 along with the squared correlation between the observed and predicted observations, $R^2 = .690$, and the root mean squared error from the fit, $s = 1.819$ (in kpsi).

The mean squared error of the fit (in the original space rather than in log space) was calculated as

$$s^2 = \sum_{i=1}^{n} (\text{MOR}_i - \hat{\text{MOR}}_i)^2/(n-p)$$

where MOR_i was the ith observed MOR value, $\hat{\text{MOR}}_i$ was the ith predicted (from the fitted model) MOR value, n equaled 590, and the number of parameters, p, for Model 1 equaled 4.

A plot of the observed MOR values against the corresponding predicted MOR values is provided in Figure 1. The straight line is the $y = x$ line.

6.2 Model 2

To fit Models 2 through 5 we performed nonlinear least squares fits. We wrote the nonlinear regression programs in the Java programming language. These programs made use of Schnabel et al.'s (1982) Uncmin nonlinear optimization package. They can be found at `http://www1.fpl.fs.fed.us/knots_2x4.html`.

The nonlinear optimizations used to fit Models 2 through 4 all require initial estimates of the powers associated with the 4 band factors (parameters β_5–β_8 for Model 2 and parameters β_6–β_9 for Models 3 and 4) associated with the compression edge band, the compression near middle band, the tension near middle band, and the tension edge band. We used 0 as the initial estimate for all these parameters.

Estimates of the parameters of Model 2 are provided in Table 4 along with the squared correlation between the observed and predicted observations, $R^2 = .827$, and the root mean squared error from the fit, $s = 1.362$ in kpsi (9.39 in MPa).

A plot of the observed MOR values against the corresponding predicted MOR values is provided in Figure 2. The straight line is the $y = x$ line.

6.3 Model 3

The nonlinear optimization used to fit Model 3 requires (as do the optimizations for Models 4 and 5) initial estimates of the new α and Q/P parameters associated with a Hankinson approach to the slope of grain factor. In line with values reported in Kretschmann (2010) we used 1.75 and .07 as initial estimates of α (β_4) and Q/P (β_5), respectively.

Estimates of the parameters of Model 3 are provided in Table 5 along with the squared correlation between the observed and predicted observations, $R^2 = .827$, and the root mean squared error from the fit, $s = 1.362$ in kpsi (9.39 in MPa).

Note that the estimated band powers (parameters 5–8 for Model 2 and 6–9 for Model 3) for Models 2 and 3 are similar. They suggest that knots near the tension edge have the greatest (reducing) effect on MOR, followed in order by knots near the compression edge, knots in the tension region near the middle of the board, and knots in the compression region near the middle of the board. (In fact, the models suggest that knots in the compression region near the center of the board might have a slight positive effect on MOR.)

Also note that the estimated α and Q/P Hankinson parameters for Models 3 through 5 exceed the values reported in Kretschmann (2010). This suggests, perhaps, that our models' incorporations of slope of grain effects could be improved.

A plot of the observed MOR values against the corresponding predicted MOR values is provided in Figure 3. The straight line is the $y = x$ line.

6.4 Model 4

Estimates of the parameters of Model 4 are provided in Table 6 along with the squared correlation between the observed and predicted observations, $R^2 = .827$, and the root mean squared error from the fit, $s = 1.358$ in kpsi (9.36 in MPa).

We note that Model 4 incorporates "band effects" (the effects of compression and tension regions) differently than do Models 2 and 3. Compare, for example,

$$(1 - p_{11})^{\beta_6} \times (1 - p_{21})^{\beta_7} \times (1 - p_{31})^{\beta_8} \times (1 - p_{41})^{\beta_9} / \beta_{10}$$

from Model 3 with

$$\begin{gathered}(1 - f_{1j} + a \times f_{1j})^{\beta_6} \\ \times (1 - f_{2j} + a \times f_{2j})^{\beta_7} \\ \times (1 - f_{3j} + a \times f_{3j})^{\beta_8} \\ \times (1 - f_{4j} + a \times f_{4j})^{\beta_9} / \text{denom}_j\end{gathered}$$

from Model 4, where the p_{ij}'s are area fractions and the f_{ij}'s are fractions of a vertical line. Despite this, the Model 4 band power parameter estimates reported in Table 6 also suggest, as do the corresponding band power estimates in Tables 4 and 5, that under third point loading, knots in the tension edge band have the greatest strength-reducing effect and that knots in the near middle compression region have the smallest strength-reducing effect.

A plot of the observed MOR values against the corresponding predicted MOR values is provided in Figure 4. The straight line is the $y = x$ line.

6.5 Model 5

Estimates of the parameters of Model 5 are provided in Table 7 along with the squared correlation between the observed and predicted observations, $R^2 = .825$, and the root mean squared error from the fit, $s = 1.365$ in kpsi (9.41 in MPa).

We note that Model 5 incorporates "band effects" (the effects of compression and tension regions) differently than does Model 4. Compare, for example,

$$\begin{gathered}(1 - f_{1j} + a \times f_{1j})^{\beta_6} \\ \times (1 - f_{2j} + a \times f_{2j})^{\beta_7} \\ \times (1 - f_{3j} + a \times f_{3j})^{\beta_8} \\ \times (1 - f_{4j} + a \times f_{4j})^{\beta_9} / \text{denom}_j\end{gathered}$$

from Model 4 with

$$\begin{gathered}(1 - f_{1j} + \beta_6 \times f_{1j})^{\beta_{10}} \\ \times (1 - f_{2j} + \beta_7 \times f_{2j})^{\beta_{10}} \\ \times (1 - f_{3j} + \beta_8 \times f_{3j})^{\beta_{10}} \\ \times (1 - f_{4j} + \beta_9 \times f_{4j})^{\beta_{10}} / \text{denom}_j\end{gathered}$$

from Model 5. Despite this, the Model 5 "strength factor" parameter estimates reported in Table 7 ($\beta_6, \ldots, \beta_9$) also suggest, as do the corresponding band power estimates in Table 6, that under third point loading, knots in the tension edge band have the greatest strength-reducing effect and that knots in the near middle compression region have the smallest strength-reducing effect. That is, in Model 5, lower values among β_6 – β_9 correspond to larger reductions in strength for a given length of knot intersection with one of the 1800 vertical lines in the grid and higher values correspond to smaller reductions in strength. Thus, the .616 value for β_9 (the tension edge band parameter) suggests the greatest reduction in strength and the .948 value for β_7 (the near middle compression band parameter) suggests the least reduction in strength.

A plot of the observed MOR values against the corresponding predicted MOR values is provided in Figure 5. The straight line is the $y = x$ line.

7 Avoiding Error Underestimation

To obtain an idea of the true predictive power of a model, it is useful to divide the data into "fitting" and "test" sets. The results reported in Tables 3–7 make use of all 590 data points and yield estimates of s, root mean squared error. However, better estimates of the error in predicting *new* data, can be obtained by dividing our 590 data points into "fitting" and "test" sets. For ten trials, we randomly selected 300 of our boards as the "fitting" set and used the remaining 290 data boards as the test set. This permitted us to obtain 10 estimated s_{test} values where

$$s^2_{\text{test}} = \sum_{i=1}^{290} (y_i - \hat{y}_i)^2/290$$

where the y_i values corresponded to the 290 boards that were *not* a part of a 300 board "fitting set," and the $\hat{y}_i$ values were the predicted values for the test set based on the fit to the fitting set.

The resulting s values are provided in Tables 8 – 11. They suggest that more conservative s values for Models 2–5 are 1.40, 1.40, 1.38, and 1.39 (in kpsi).

8 Comparing Our s Values with s Values from Other Studies

We have s values for 5 of the 9 models listed in Table 1b. Two of these s values fall above our s values. Two fall below. This may reflect reality, or, as discussed in Section 2, the ordering might be clouded by differences in species, board sizes, board grades, and moisture content variability and a failure to test fits on *new* sets of data (or, alternatively, to perform cross-validations).

9 Further Work

We have also developed software that permits us to estimate rings per inch, percentage of latewood, distance to pith, and location on a flatsawn to quartersawn spectrum from images of endpieces cut from the boards in our mill run data sets. We intend to analyze the endpieces via this software and to determine whether any of these additional predictors improve our model. (We realize that some of the new predictors might be highly correlated with, for example, specific gravity, and thus might add little predictive power to our current model.) In addition, we intend to perform a careful investigation of those specimens that are associated with larger residuals to determine whether we can identify additional predictors that should be added to our model (for example, machine damage, shake, wane, knot type, ...).

10 Potential Cost of Failing to Predict Strength Accurately

In the United States, it is well-recognized that our practice of setting the bending strength allowable property of a visual grade of lumber equal to (essentially) the 5th percentile of that grade divided by 2.1 yields, for the sake of safety, an inefficient process. In part we are currently "forced" to act inefficiently because, at the moment, we cannot predict the strength of individual boards with sufficient accuracy. In this section, we discuss two analyses that help us begin to evaluate the potential cost of failing to predict strength sufficiently accurately.

10.1 Is an allowable property approach wasteful?

In Figures 6–9 we plot observed MOR values versus predicted MOR values for Models 2–5 and **No. 2 data**. We also plot

- the $y = x$ line (so the vertical distance between a point and the line is a $y_{\text{observed}} - y_{\text{predicted}}$ value, a residual)
- the 3 lines $y_{\text{predicted},i} - 2 \times s$ versus $y_{\text{predicted},i}$, $y_{\text{predicted},i} - 3 \times s$ versus $y_{\text{predicted},i}$, and $y_{\text{predicted},i} - 4 \times s$ versus $y_{\text{predicted},i}$, where $s = \sqrt{\sum_{i=1}^{n} (y_{\text{observed},i} - y_{\text{predicted},i})^2/(n-p)}$ (p is the number of parameters in the model) is a measure of the uncertainty in the model prediction
- the line $y_{\text{predicted},i} - 4 \times s_{\text{Olsson}}$ versus $y_{\text{predicted},i}$ where s_{Olsson} is two-thirds of our s and reflects the ratio between Olsson et al.'s 6.3 s value (in MPa) in Table 1b and our 9.4 (in MPa) in Table 1b.

For Figures 6 – 9, the s values (in kpsi) are the bottom right values (1.399, 1.404, 1.378, and 1.385) in Tables 8 – 11.

We know that if the errors (roughly equivalent to the residuals in our model: the $y_{\text{observed}} - y_{\text{predicted}}$ values) are normally distributed, then only approximately .023 of the predicted MOR, actual MOR pairs will fall below the $2 \times s$ line, only approximately .0017 of the pairs will fall below the $3 \times s$ line, and only approximately .00003 of the pairs will fall below the $4 \times s$ line. Thus we can be assured that if errors are normally distributed, then for boards with a predicted strength value above the x value at which the horizontal allowable property line intersects the $y_{\text{predicted}}(x) - 4 \times s$ versus x line, the actual strength value will be above the allowable property and as the predicted MOR increases, *much* above the allowable property (with *high* probability). Shapiro-Wilk tests do not reject normality for the residuals from Models 2 and 3. (The p-values were 0.87 and 0.89, respectively.) Shapiro-Wilk tests cast greater doubt on normality for the residuals from Models 4 and 5. (The p-values were 0.052 and 0.038, respectively.)

Consider Model 3. In Table 9 we report that a reasonable estimate of the s value for Model 3 is 1.404. We use 1.26 kpsi as the allowable property value for No. 2 Southern Pine 2×4 lumber. (This corresponds to an adjustment of the 1.1 kpsi value appropriate for 144-inch lumber lengths to a value appropriate for the 59.5-inch "length" in our third point tests. See section 8.4.3 in ASTM D1990.) Thus the x coordinate of the intersection point of the horizontal $y = 1.26$ allowable property line in Figure 7 with the diagonal $y = x - 4 \times s$ line is given by $1.26 = x - 4 \times 1.404$. That is, the intersection point is (6.876,1.26). 78 of the 176 data points (about 44%) have predicted MOR values that lie above the 6.876 value. This leads to many boards with ".99997 probability lower bounds" on their strength that are well above the allowable property.

If the Olsson et al. results were applicable to Southern Pine, then the plots of observed MOR values versus predicted MOR values would be even tighter, and the ".99997 probability lower limit line" would lie along the "Olsson" lines in Figures 6 – 9. Actually there will be sample and model uncertainty associated with this ".99997" line, but it remains clear that much higher strength values could be assumed (for high enough predicted strengths) than the allowable property value.

Of course, an MOR allowable property is also designed to take into account a combination of "duration of load" and "safety adjustment" factors via the 2.1 divisor, which complicates this critique of a single 5th/2.1 allowable property shared across a visual grade. We can get a rough idea of the effect of such factors when we are predicting the strengths of individual boards by considering Figure 10. Figure 10 is based on Model 3 (as is Figure 7). However, rather than plotting $y = x - 2 \times s$, $y = x - 3 \times s$, and $y = x - 4 \times s$ lines for individual predicted board MOR values, we can calculate

1. the $y = (x - 2 \times s)/1.6$ line
2. the $y = (x - 3 \times s)/1.6$ line
3. the $y = (x - 4 \times s)/1.6$ line
4. the $y = (x - 1.645 \times s)/2.1$ line

The $y = (x - 1.645 \times s)/2.1$ line is roughly in accord with current allowable property practices except that it uses $x - 1.645 \times s$ as an estimate of the 5th percentile of the local (for predicted strength near x) strength distribution (and it uses this estimate of the 5th percentile of the local strength distribution rather than a lower confidence bound on this 5th percentile). The 2.1 factor is composed of a 1.6 duration of load factor and a 1.3 safety factor.

The $y = (x - 2 \times s)/1.6$, $y = (x - 3 \times s)/1.6$, and $y = (x - 2 \times s)/1.6$ lines include the 1.6 duration of load factor, but incorporate "safety factors" via the 2, 3, and 4 multipliers so that we begin with estimates of 2.3, .17, or .003 percentiles rather than with an estimate of a 5th percentile.

We are not currently proposing any of these lines as alternatives to any current standards. We do claim that our analyses suggest that it is not efficient for boards from the upper and lower ends of the No. 2 grade to share a single common allowable property. Again, we note that this kind of observation is not a revelation to wood scientists. However, our analysis has made it somewhat more quantitative.

10.2 "Flipping a board"

As quantified (to some extent) in this paper, wood scientists know that knots near the tension edge of a board under a bending load reduce the strength of that board more than the "same" knots near the compression edge (Kretschmann, 2010). Thus, if one knew that a board were going to be placed under a bending load in a structure, it would make sense (if it were sufficiently inexpensive, and the benefit were sufficiently high) to identify the edge of the board that

should be placed under tension. (Of course one must always balance the need for efficient use of material with the need for user friendliness for the installer.)

Our current models are not good enough to guarantee that we have a precise measure of the difference in the bending strengths of the two possible configurations of a board. However, our models do permit us to obtain a rough idea of the gains that might be made by identifying the "best tension edge." In Figure 11, using Model 3, we plot the larger predicted strength of a board versus the smaller predicted strength of a board. As one would expect, for stronger boards (boards with fewer, smaller knots), there is little (or no) difference between the two configurations. However, for weaker boards (with more, larger knots), the difference can amount to a significant fraction of the board's strength. This point is made in greater detail in Figure 12. It suggests, for example, that many boards with a minimum predicted bending strength around 5 kpsi, can have a maximum bending strength 10% to 20% higher (and sometimes nearly 40% higher) if flipped. The frequencies of various strength increases (with a flip of a board) are presented in Figure 13. In Figures 14, 15, and 16 we provide the corresponding plots for Model 4.

If we can improve our models and further reduce the corresponding s values (reduce the uncertainties in our estimated strengths), and if our estimates of the benefits of a board flip are large enough, and the costs of marking a recommended tension edge are small enough (and if carpenters can be convinced that flipping is useful), then such marking and associated special marketing might be justified.

10.2.1 Aside 1

As mentioned in Section 2, we note that Olsson et al.'s (2017) model could be modified to incorporate an ability to yield different predicted board strengths depending on which edge is under tension in a bending scenario. A simple modification might be, for example,

$$\text{Predicted strength} = C \times \min_j F_j \tag{14}$$

where $C, \beta_1, \beta_2, \beta_3, \beta_4$ are parameters to be fit (via least squares) and

$$F_j = (E_{1j}/E)^{\beta_1} \times (E_{2j}/E)^{\beta_2} \times (E_{3j}/E)^{\beta_3} \times (E_{4j}/E)^{\beta_4} \tag{15}$$

where the minimum is taken over their series of vertical lines across a board, E is a global measure of stiffness, and $E_{1j}, E_{2j}, E_{3j}, E_{4j}$ are their local measures of stiffness in the upper (compression edge) band, upper middle (compression region next to mid-line) band, lower middle (tension region next to mid-line) band, and lower (tension edge) band in the jth vertical line across the board.

10.2.2 Aside 2

We further note that European standards currently appear to mandate (at least indirectly) that acceptable models not yield significantly different predicted strengths for a piece of lumber when compression and tension edges are switched. See the discussion of "repeatability checks" and "different passes through the scanner" above table 3 in Olsson et al. (2017) and in section 5.2 of Olsson et al. (2017). Also see Lukacevic et al.'s (2015) discussion of this issue in their Conclusion section. If this is the case, the European standards might need to be modified so that models would be permitted to predict bending strength changes when tension and compression edges are switched.

The standards could still require that the *pair* of predicted bending strength values (corresponding to the two possible bending edges) not change significantly regardless of how a board is fed through a scanning/prediction device.

11 Summary

We have developed a Java-based image analysis program that permits us to obtain knot estimates from a large collection of images of mill run Southern Pine 2×4's. These images are accompanied by a large data set that includes information on MOR measured under third point loading, modulus of elasticity (and other measures of stiffness), specific gravity, and slope of grain. We have also developed nonlinear least squares programs that permit us to fit four related nonlinear models that predict MOR as a function of MOE, SG, SOG, and knot information. These models permit us to predict MOR (under third point loading) with approximately a 1.4 kpsi root mean squared error. (We hope via outlier analysis and the consideration of additional information available from images — e.g., machine damage, shake, knot type, ... — to further reduce this value.)

We will be obtaining additional predictors (rings per inch, percent latewood, distance to pith, and location on a flatsawn to quartersawn spectrum) via a second Java-based image analysis program, and hope to incorporate this information into an improved model.

We have reported analyses that suggest that even our current 1.4 kpsi root mean squared error is small enough to permit more efficient "quality binning/categorization" of lumber. However, any such binning will also require more detailed knowledge of the loads to which particular bins of boards will be subjected (they will not, of course, be subjected to third point loading in actual structures).

Further, for our research to be commercially implemented, our "human-based" image analysis methods and "human-based" SOG measurements will need to be replaced by high-speed machine measurements. Such devices, or similar ones based on related technology, are already being deployed commercially for the purposes of "machine grading."

12 References

Anderson, G.C., Owens, F.C., Verrill, S.P., Ross, R.J., and Shmulsky, R. (2021), "Fitting Statistical Distribution Models to MOE and MOR in Mill-Run Spruce and Red Pine Lumber Populations," *Wood and Fiber Science*, **53**(1), pp. 17-26.

Barbosa, M.C., Street, J., Owens, F.C., Shmulsky, R. (2019), "The Effect of Multiple Knots in Close Proximity on Southern Pine Lumber Properties," *Forest Products Journal*, **69**(4), pp. 278-282.

Cao, Y., Street, J., Mitchell, B., To, Filip, DuBien, Janice, Seale, R.D., Shmulsky, R. (2018), "Effect of Knots on Horizontal Shear Strength in Southern Yellow Pine," *BioResources*,**13**(2), pp. 4509-4520.

França, F.J.N., Seale, R.D., Shmulsky, R., and França, T.S.F.A. (2019), "Modeling Mechanical Properties of 2 by 4 and 2 by 6 Southern Pine Lumber Using Longitudinal Vibration and Visual Characteristics," *Forest Products Journal*, **68**(3), pp. 286-294.

Hanhijärvi, A. and Ranta-Maunus, A. (2008), Development of strength grading of timber using combined measurement techniques. Report of the Combigrade-project – phase 2. Espoo. VTT Publications 686, 55 pages.

Hietaniemi, R., López, M.B., Hannuksela, J., Silvén, Olli (2014), "A Real-Time Imaging System for Lumber Strength Prediction", *Forest Products Journal*, **64**(3/4), pp. 126-133.

Kretschmann, D.E. (2010), "Mechanical Properties of Wood" and "Stress Grades and Design Properties for Lumber, Round Timber, and Ties," Chapters 5 and 7 in *Wood Handbook — Wood as an Engineering Material*, General Technical Report FPL-GTR-190, Madison, WI: U.S. Department of Agriculture, Forest Service, Forest Products Laboratory, 508 pages.

Lukacevic, M., Füssl, J., and Eberhardsteiner, J. (2015), "Discussion of common and new indicating properties for the strength grading of wooden boards," *Wood Sci Technol*, **49**, pp. 551-576.

Olsson, A., Oscarsson, J., Serrano, E., Källsner, B., Johansson, M., and Enquist, B. (2013), "Prediction of timber bending strength and in-member cross-sectional stiffness variation on the basis of local wood fibre orientation," *Eur. J. Wood Prod.*, **71**, pp. 319-333.

Olsson, A. and Oscarsson, J. (2017), "Strength grading on the basis of high resolution laser scanning and dynamic excitaton: a full scale investigation of performance," *Eur. J. Wood Prod.*, **75**, pp. 17-31.

Owens, F.C, Verrill, S.P., Shmulsky, R., and Kretschmann, D.E. (2018), "Distributions of MOE and MOR in a Full Lumber Population," *Wood and Fiber Science*, **50**(3), pp. 265-279.

Owens, F.C, Verrill, S.P., Shmulsky, R., and Ross, R.J. (2019), "Distributions of Modulus of Elasticity and Modulus of Rupture in Four Mill-Run Lumber Populations," *Wood and Fiber Science*, **51**(2), pp. 183-192.

Owens, F.C, Verrill, S.P., Shmulsky, R., and Ross, R.J. (2020), "Distributions of MOE and MOR in Eight Mill-Run Lumber Populations (Four Mills at Two Times)," *Wood and Fiber Science*, **52**(2), pp. 165-177.

R Core Team (2018). R: A language and environment for statistical computing. R Foundation for Statistical Computing, Vienna, Austria. URL https://www.R-project.org/.

Schajer, G.S (2001), "Lumber Strength Grading Using X-ray Scanning," *Forest Products Journal*, **51**(1), pp. 43-50.

Schnabel, R.B., Koontz, J.E., and Weiss, B.E. (1982), *A Modular System of Algorithms for Unconstrained Minimization*, Report CU-CS-240-82, Comp. Sci. Dept., University of Colorado at Boulder.

Verrill, S.P., Evans, J.W., Kretschmann, D.E., and Hatfield, C.A. (2012). "Asymptotically Efficient Estimation of a Bivariate Gaussian–Weibull Distribution and an Introduction to the Pseudo-truncated Weibull." Research Paper FPL-RP-666. Madison, WI: U.S. Department of Agriculture, Forest Service, Forest Products Laboratory. 76 pages.

Verrill, S.P., Evans, J.W., Kretschmann, D.E., and Hatfield, C.A. (2013). "An Evaluation of a Proposed Revision of the ASTM D 1990 Grouping Procedure." Research Paper FPL-RP-671. Madison, WI: U.S. Department of Agriculture, Forest Service, Forest Products Laboratory. 34 pages.

Verrill, S.P., Evans, J.W., Kretschmann, D.E., and Hatfield, C.A. (2014), "Reliability Implications in Wood Systems of a Bivariate Gaussian–Weibull Distribution and the Associated Univariate Pseudo-truncated Weibull," *ASTM Journal of Testing and Evaluation*, **42**, Number 2, pp. 412-419.

Verrill, S.P., Evans, J.W., Kretschmann, D.E., and Hatfield, C.A. (2015), "Asymptotically Efficient Estimation of a Bivariate Gaussian–Weibull Distribution and an Introduction to the Pseudo-truncated Weibull," *Communications in Statistics – Theory and Methods*, **44**, pp. 2957-2975.

Verrill, S.P., Owens, F.C., Kretschmann, D.E., and Shmulsky, R. (2017). "Statistical Models for the Distribution of Modulus of Elasticity and Modulus of Rupture in Lumber with Implications for Reliability Calculations." Research Paper FPL-RP-692. Madison, WI: U.S. Department of Agriculture, Forest Service, Forest Products Laboratory. 51 pages.

Verrill, S.P., Owens, F.C., Kretschmann, D.E., and Shmulsky, R. (2018). "A Fit of a Mixture of Bivariate Normals to Lumber Stiffness–Strength Data." Research Paper FPL-RP-696. Madison, WI: U.S. Department of Agriculture, Forest Service, Forest Products Laboratory. 44 pages.

Verrill, S.P., Owens, F.C., Kretschmann, D.E., Shmulsky, R., and Brown, L.S. (2019). "Visual and MSR Grades of Lumber Are Not 2-Parameter Weibulls and Why It Matters (With a Discussion of Censored Data Fitting)." Research Paper FPL-RP-703. Madison, WI: U.S. Department of Agriculture, Forest Service, Forest Products Laboratory. 40 pages.

Verrill, S.P., Owens, F.C., Kretschmann, D.E., Shmulsky, R., and Brown, L.S. (2020a). "Visual and MSR Grades of Lumber Are Not 2-Parameter Weibulls and Why This May Matter," *ASTM Journal of Testing and Evaluation*, **48**, Number 5, pp. 3946-3962.

Verrill, S.P., Owens, F.C., Arvanitis, M.A., Kretschmann, D.E., Shmulsky, R., Ross, R.J., and Lebow, P. (2020b). "Estimated Probability of Breakage of Lumber of a Fixed 'Grade' Can Vary Greatly from Mill to Mill and Time to Time." Research Paper FPL-RP-705. Madison, WI: U.S. Department of Agriculture, Forest Service, Forest Products Laboratory. 47 pages.

Verrill, S.P., Owens, F.C., Shmulsky, R., and Ross, R.J. (2021). "A Java Image Analysis Program for Lumber Knots, and Related Nonlinear Least Squares Routines for Fitting Lumber Modulus of Rupture to Strength Predictors." Draft research paper, Madison, WI: U.S. Department of Agriculture, Forest Service, Forest Products Laboratory. `https://www1.fpl.fs.fed.us/knots_2x4.html`

Wright, S., Dahlen, J., Montes, C., Eberhardt, T.L. (2019), "Quantifying knots by image Analysis and modeling their effects on the mechanical properties of loblolly pine Lumber," *European Journal of Wood and Wood Products*, **77**, pp. 903-917.

First Author	Date	Predictors	Technology	Special Features	Model	Bending Response	Test
Barbosa	2019	flatwise MOE, density, and knot cross-section of largest knot or knot cluster	Digimizer image analysis software that requires human interaction to identify and measure knots	Only knots between load heads/ Only largest knot or largest cluster/ Spike knots handled differently	linear	flatwise MOR	third-point (load heads at 1/3, 2/3 locations)
Franca	2019	dynamic MOE, SG, knot diameter ratio		Knots within the the test span were considered	linear	edgewise MOR	third-point (load heads at 1/3, 2/3 locations)
Hietaniemi	2014	local grain deviation and scaled size of largest knot	machine vision, GPUs, Inx, Ltd. Optigrader (knots)	All 4 faces/ only largest knot	—	edgewise MOR	3-point (load head at 1/2 location)
Lukacevic	2015	KAR, FAR, knot area on surfaces, knot interface area, knot volume, modifications of variables based on closeness to tension edge	X-ray scanner, laser scanner, computerized tomography scan	Predictors (IPs) that discount (sometimes completely) knots in the compression half	linear	edgewise MOR	third-point (load heads at 1/3, 2/3 locations)
Olsson	2013	resonance frequency of first longitudinal mode of vibration & fiber orientation	tracheid effect, WoodEye Scanner (Innovativ Vision AB)	Takes into account stress differences between the middle and outer thirds of the board length	linear	edgewise MOR	third-point (load heads at 1/3, 2/3 locations)
Olsson	2017	resonance frequency of first longitudinal mode of vibration & fiber orientation	tracheid effect, WoodEye 5 Scanner (WoodEye AB), Precigrader (Dynalyse)		linear	edgewise MOR	third-point (load heads at 1/3, 2/3 locations)

Table 1a: Previous studies, columns 1-8

First Author	Date	Predictors	Technology	Special Features	Model	Bending Response	Test
Schajer	2001	local density	X-ray scanner	Load span chosen to contain the most serious defect/Calculation limited to area that was significantly loaded	nonlinear	edgewise MOR	third-point (load heads at 1/3, 2/3 locations)
Verrill	this study	edgewise MOE, SG, slope of grain, functions of local knot areas and local knot cross-sections	Java image analysis program that requires human interaction to identify and measure knots	Takes into account stress differences among board regions/All knots between supports	nonlinear	edgewise MOR	third-point (load heads at 1/2, 2/3 locations)
Wright	2019	SG, acoustic velocity, and knot area percents	k-means clustering to identify knots	The region in which knots are counted is chosen to minimize MSE	linear	edgewise MOR	third-point (load heads at 1/2, 2/3 locations)

Table 1a continued: Previous studies, columns 1-8

First Author	Date	Species	Data Set	Number of Specimens	MC (%)	R^2	s
Barbosa	2019	Southern Yellow Pine	2×4 MOR min = 12.3 MPa MOR max = 74.7 MPa	278	conditioned to: 12%	.702	—
Franca	2019	Southern Yellow Pine	2×4 – 542 2×6 – 502 No. 2	1044	mean: 11.4%, conditioned at 22 deg C, 61% RH	.470	14.45 MPa
Hietaniemi	2014	Scots Pine	2×4 MOR min = 8.1 MPa MOR max = 71.7 MPa	194	range: 9.0% - 13.6%	.63	—
Lukacevic	2015	Norway Spruce	10 45 mm x 144 mm 8 45 mm X 189 mm 25 40 mm x 115 mm or 40 mm x 145 mm or 40 mm x 185 mm	43		.89	—
Olsson	2013	Norway Spruce	Actual 45 mm x 145 mm x 3600 mm 61 pieces met TR26 UK standard, 44 did not	105	conditioned at 20 deg C, 65% RH	.71	—
Olsson	2017	Norway Spruce	900 pieces, 9 locations (in Norway, Sweden, Finland), 10 board sizes	900	dried with a target moisture content of 12%	.70	6.3MPa

Table 1b: Previous studies, columns 9-16

First Author	Date	Species	Data Set	Number of Specimens	MC (%)	R^2	s
Schajer	2001	Southern Yellow Pine	2×4 mill run	136		.78	12.1 MPa
Verrill	this study	Southern Yellow Pine	2×4 3 mill run samples, each of approximate size 200	590	mean: 12.8% MOE, MOR adjusted to 15% MC	.827	9.4 MPa (9.65 when applied to new data)
Wright	2019	Loblolly Pine	72 2×6 (13 No. 1, 59 No. 2) 99 2×8 (59 No. 1, 40 No. 2)	171	mean: 11.2%	.65	7.2 MPa

Table 1b continued: Previous studies, columns 9-16

p_{11}	p_{12}	p_{13}	p_{14}	p_{15}	p_{16}
p_{21}	p_{22}	p_{23}	p_{24}	p_{25}	p_{26}
p_{31}	p_{32}	p_{33}	p_{34}	p_{35}	p_{36}
p_{41}	p_{42}	p_{43}	p_{44}	p_{45}	p_{46}

Table 2: Board region geometry. The board (between the two support locations) is divided into 6 columns of 4 rows (or 24 "cells"). The columns are of equal width. The rows are of equal height. Columns 3 and 4 correspond to the region between the two load points. Row 1 includes the compression edge. Row 4 includes the tension edge. For $i \in \{1, 2, 3, 4\}$ and $j \in \{1, 2, 3, 4, 5, 6\}$, p_{ij} is the fraction of the area in cell i, j that lies in a knot.

Parameter ID	Value
β_1 (constant)	.040
β_2 (MOE)	.995
β_3 (SG)	.530
β_4 (SOG)	1.208
R^2	.690
s_{590}	1.819

Table 3: Parameter estimates for Model 1, together with the corresponding R^2 and root mean squared error (in kpsi) values. s_{590} is the root mean squared error with five outliers removed.

Parameter ID	Value
β_1 (constant)	.883
β_2 (MOE)	.707
β_3 (SG)	.615
β_4 (SOG)	.563
β_5 (band 1 power)	1.282
β_6 (band 2 power)	-.137
β_7 (band 3 power)	1.052
β_8 (band 4 power)	3.048
β_9 (cols 1,6 divisor)	.257
β_{10} (cols 2,5 divisor)	.901
R^2	.827
s_{590}	1.362
s_{593}	1.389
s_{above4}	1.363
s_{above3}	1.365

Table 4: Parameter estimates for Model 2, together with the corresponding R^2 and root mean squared error (in kpsi) values. s_{590} is the root mean squared error with five outliers removed. s_{593} is the root mean squared error with the three identified "machine damage" outliers added back to the data set. s_{above4} is the root mean squared error for No. 3 and above lumber with the one identified No. 3 and above "machine damage" outlier added back to the data set. s_{above3} is the root mean squared error for No. 2 and above lumber. (There were no identified No. 2 and above "machine damage" outliers.) The parameter estimates and R^2 are from the 590 data point fit.

Parameter ID	Value
β_1 (constant)	10.602
β_2 (MOE)	.707
β_3 (SG)	.611
β_4 (α)	2.136
β_5 (Q/P)	.450
β_6 (band 1 power)	1.286
β_7 (band 2 power)	-.141
β_8 (band 3 power)	1.035
β_9 (band 4 power)	3.050
β_{10} (cols 1,6)	.259
β_{11} (cols 2,5)	.901
R^2	.827
s_{590}	1.362
s_{593}	1.388
s_{above4}	1.363
s_{above3}	1.361

Table 5: Model 3. See Table 4 for an explanation of the table entries.

Parameter ID	Value
β_1 (constant)	9.767
β_2 (MOE)	.680
β_3 (SG)	.478
β_4 (α)	2.506
β_5 (Q/P)	.448
β_6 (band 1 power)	.515
β_7 (band 2 power)	.170
β_8 (band 3 power)	.716
β_9 (band 4 power)	1.563
a or β_{10} (knot "strength" factor)	.553
R^2	.827
s_{590}	1.358
s_{593}	1.385
s_{above4}	1.339
s_{above3}	1.334

Table 6: Parameter estimates for Model 4, together with the corresponding R^2 and root mean squared error (in kpsi) values. s_{590} is the root mean squared error with five outliers removed. s_{593} is the root mean squared error with the three identified "machine damage" outliers added back to the data set. s_{above4} is the root mean squared error for No. 3 and above lumber with the one identified No. 3 and above "machine damage" outlier added back to the data set. s_{above3} is the root mean squared error for No. 2 and above lumber. (There were no identified No. 2 and above "machine damage" outliers.) The parameter estimates and R^2 are from the 590 data point fit.

Parameter ID	Value
β_1 (constant)	9.631
β_2 (MOE)	.685
β_3 (SG)	.459
β_4 (α)	2.525
β_5 (Q/P)	.443
β_6 (str fac 1)	.869
β_7 (str fac 2)	.948
β_8 (str fac 3)	.802
β_9 (str fac 4)	.616
β_{10} (power)	1.869
R^2	.825
s_{590}	1.365
s_{593}	1.390
s_{above4}	1.344
s_{above3}	1.336

Table 7: Model 5. See Table 6 for an explanation of the table entries.

Fitted Model	s for fitted 590	s for fitted 300	s for predicted 290
Full 590	1.362		
300, 1		1.336 *	1.417
300, 2		1.375 *	1.462
300, 3		1.382 *	1.388
300, 4		1.385	1.299 *
300, 5		1.440	1.340 *
300, 6		1.301 *	1.400
300, 7		1.336 *	1.499
300, 8		1.298 *	1.410
300, 9		1.278 *	1.417
300, 10		1.305 *	1.353
mean of 10		1.344	1.399

Table 8: Model 2 (fraction of area, 4 rows, 6 columns, non-Hankinson SOG) s values (in kpsi). * indicates lower value in row.

Fitted Model	s for fitted 590	s for fitted 300	s for predicted 290
Full 590	1.362		
300, 1		1.339 *	1.418
300, 2		1.379 *	1.464
300, 3		1.372 *	1.410
300, 4		1.389	1.302 *
300, 5		1.498	1.358 *
300, 6		1.301 *	1.412
300, 7		1.338 *	1.493
300, 8		1.301 *	1.408
300, 9		1.281 *	1.419
300, 10		1.307 *	1.356
mean of 10		1.351	1.404

Table 9: Model 3 (fraction of area, 4 rows, 6 columns, Hankinson SOG) s values (in kpsi). * indicates lower value in row.

Fitted Model	s for fitted 590	s for fitted 300	s for predicted 290
Full 590	1.358		
300, 1		1.389	1.315 *
300, 2		1.291 *	1.417
300, 3		1.382 *	1.478
300, 4		1.325 *	1.350
300, 5		1.392	1.288 *
300, 6		1.333 *	1.425
300, 7		1.305 *	1.435
300, 8		1.380	1.346 *
300, 9		1.342 *	1.358
300, 10		1.297 *	1.368
mean of 10		1.344	1.378

Table 10: Model 4 (fraction of vertical line, 4 rows, 1800 vertical lines, Hankinson SOG, 1 strength factor, 4 powers) s values (in kpsi). * indicates lower value in row.

Fitted Model	s for fitted 590	s for fitted 300	s for predicted 290
Full 590	1.365		
300, 1		1.401	1.325 *
300, 2		1.293 *	1.423
300, 3		1.381 *	1.474
300, 4		1.327 *	1.355
300, 5		1.400	1.296 *
300, 6		1.340 *	1.439
300, 7		1.306 *	1.439
300, 8		1.392	1.355 *
300, 9		1.355 *	1.366
300, 10		1.301 *	1.375
mean of 10		1.350	1.385

Table 11: Model 5 (fraction of vertical vertical line, 4 rows, 1800 vertical lines, Hankinson SOG, 4 strength factors, 1 power) s values (in kpsi). * indicates lower value in row.

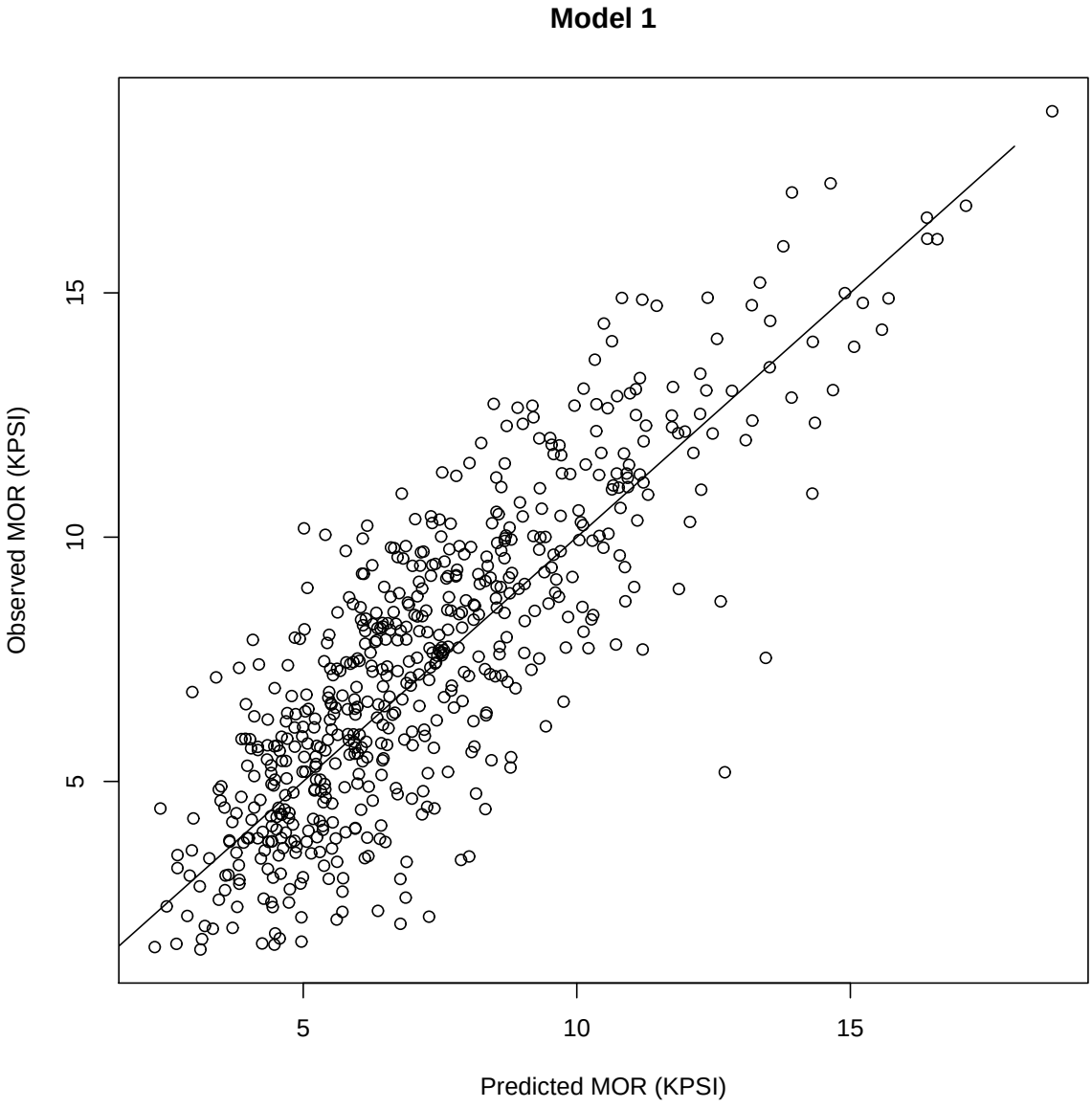

Figure 1: Model 1. Non-Hankinson SOG factor. No knot factor. A plot of the observed MOR values against the corresponding predicted MOR values. The straight line is the $y = x$ line. $s = 1.819$.

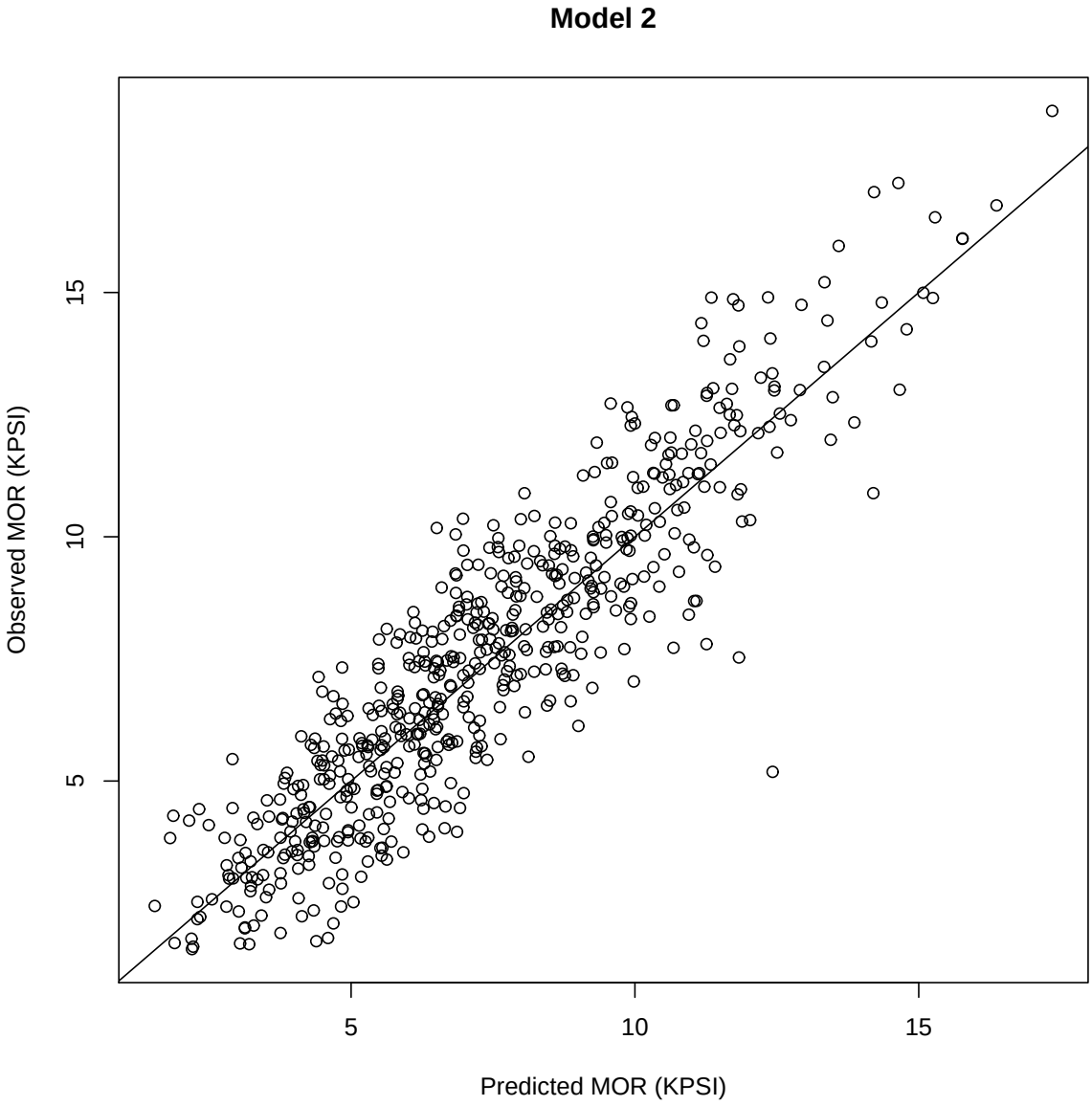

Figure 2: Model 2. Non-Hankinson SOG factor. Knot factor based on knot areas on wide faces ("non-KAR"). A plot of the observed MOR values against the corresponding predicted MOR values. The straight line is the $y = x$ line. s = 1.362.

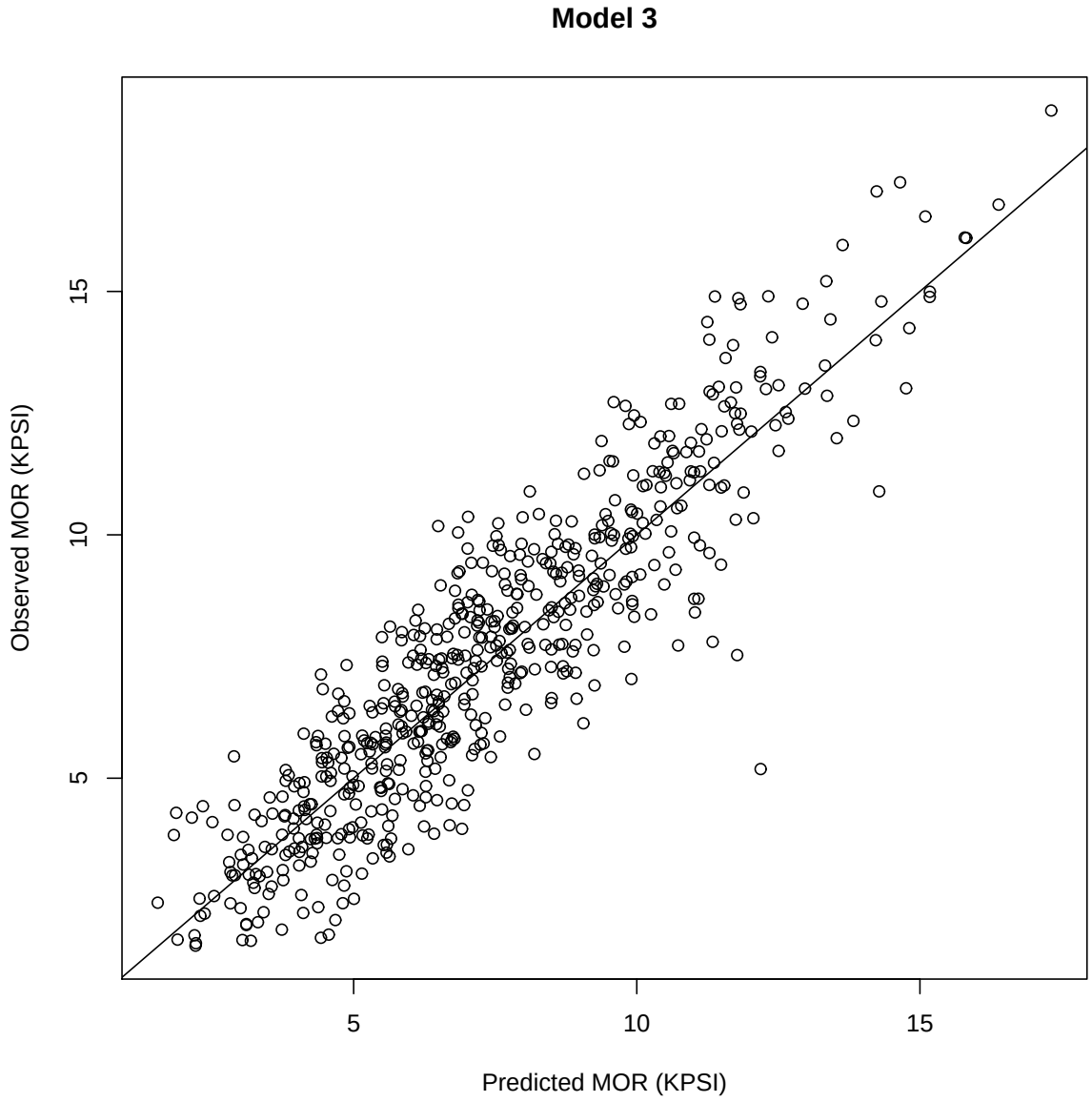

Figure 3: Model 3. Hankinson SOG factor. Knot factor based on knot areas on wide faces ("non-KAR"). A plot of the observed MOR values against the corresponding predicted MOR values. The straight line is the $y = x$ line. $s = 1.362$.

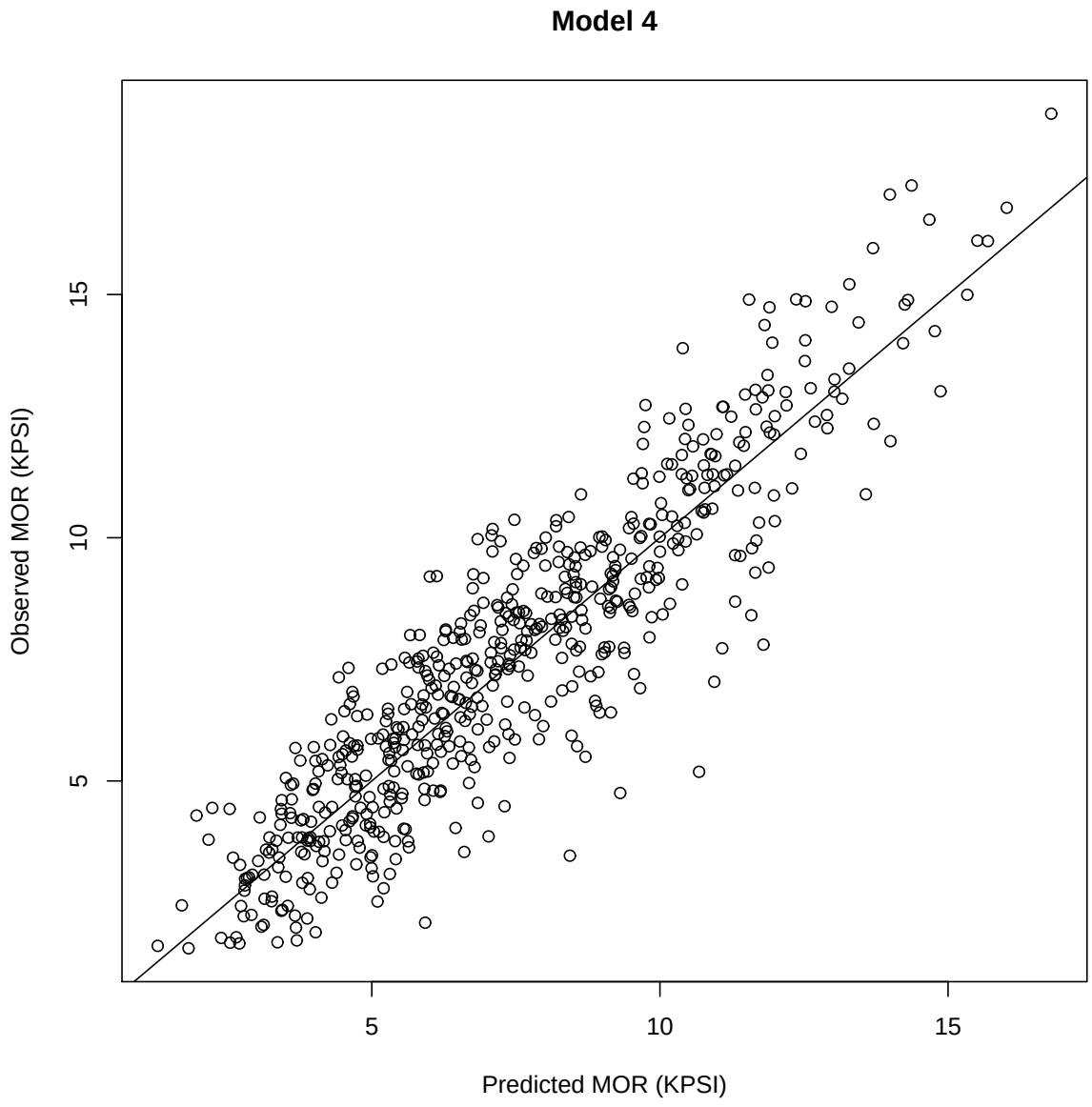

Figure 4: Model 4. Hankinson SOG factor. Knot factor based on vertical "heights" on wide faces ("KAR" approach 1). A plot of the observed MOR values against the corresponding predicted MOR values. The straight line is the $y = x$ line. $s = 1.358$.

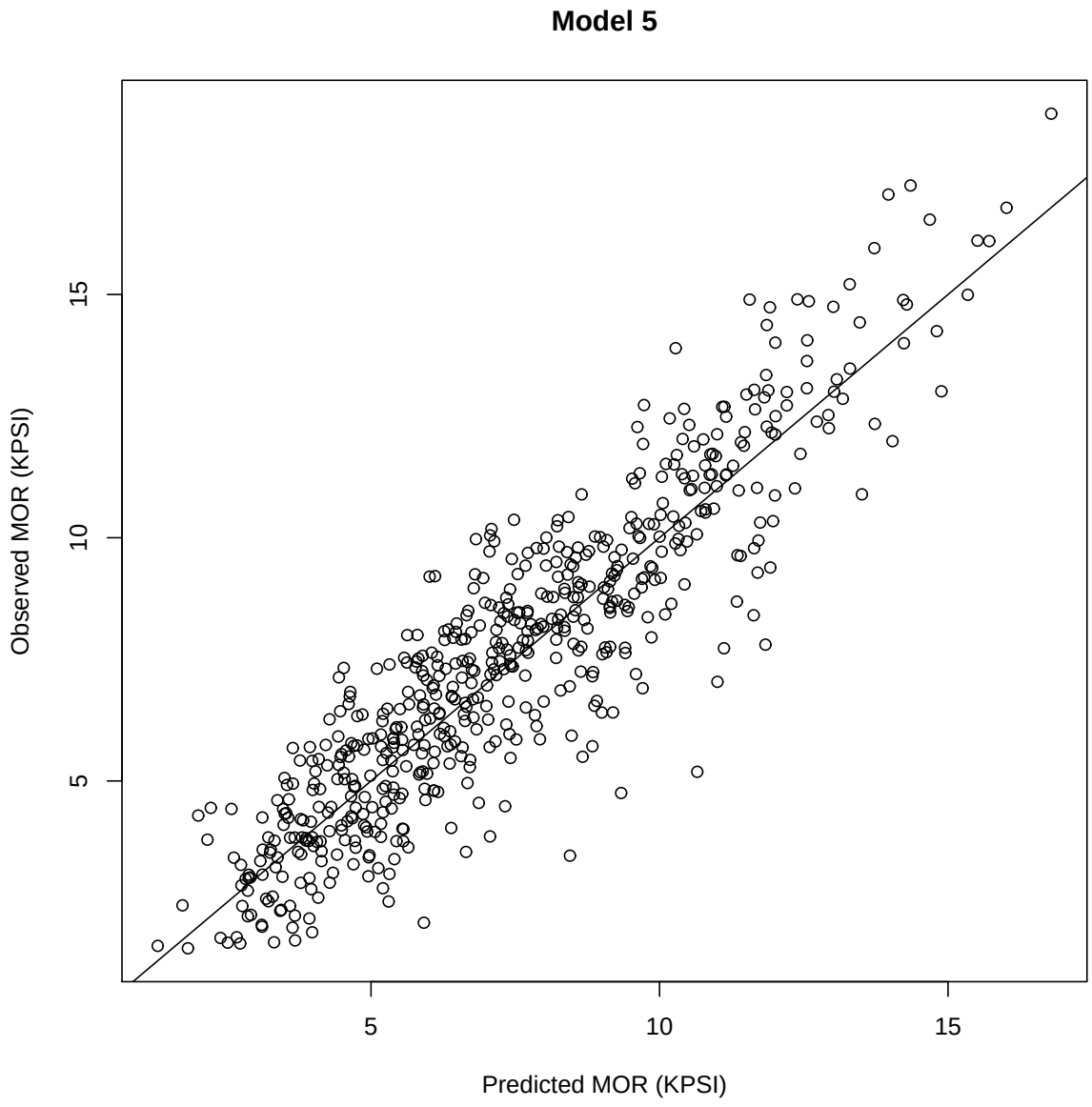

Figure 5: Model 5. Hankinson SOG factor. Knot factor based on vertical "heights" on wide faces ("KAR" approach 2). A plot of the observed MOR values against the corresponding predicted MOR values. The straight line is the $y = x$ line. $s = 1.365$.

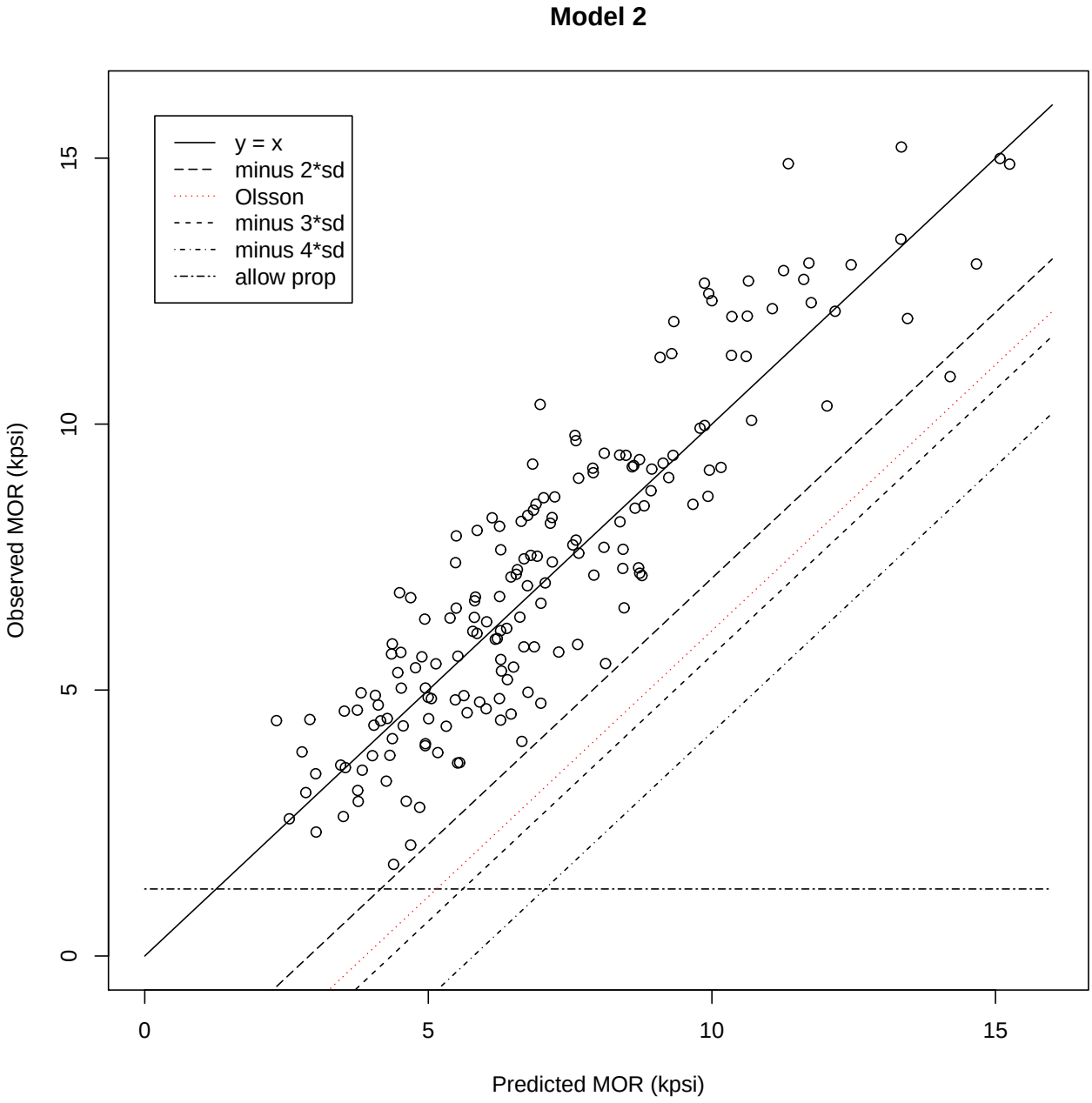

Figure 6: Plot of Model 2 observed versus predicted MORs together with $y = x$, $y = x - 2 \times s$, $y = x - 3 \times s$, $y = x - 4 \times s$, and $y = 1.26$ lines. Only **No. 2 data** is plotted. (Here we use 1.26 kpsi as the allowable property value for No. 2 Southern Pine 2x4 lumber. This corresponds to an adjustment of the 1.1 kpsi value appropriate for 144 inch lumber lengths to a value appropriate for the 59.5 inch "length" in our third point tests. See section 8.4.3 in ASTM D1990.) The plot also contains a line labeled "Olsson". The "Olsson" line is the $y = x - 4 \times s_{\text{Olsson}}$ line where the s_{Olsson} value is two-thirds of our s value and reflects Olsson *et al.*'s 6.30 Mpa s estimate.

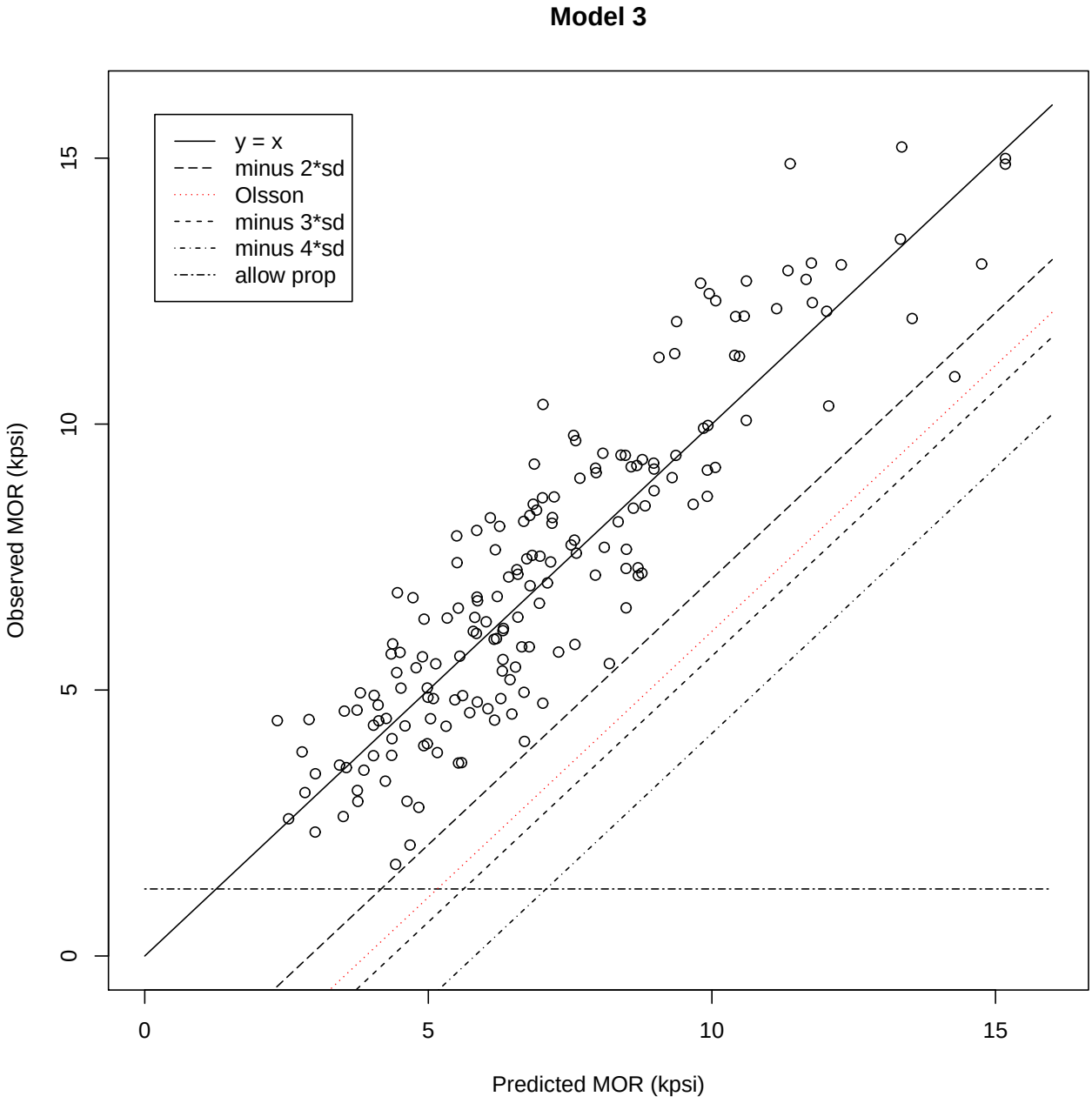

Figure 7: Plot of Model 3 observed versus predicted MORs together with $y = x$, $y = x - 2 \times s$, $y = x - 3 \times s$, $y = x - 4 \times s$, and $y = 1.26$ lines. Only **No. 2 data** is plotted. (Here we use 1.26 kpsi as the allowable property value for No. 2 Southern Pine 2x4 lumber. This corresponds to an adjustment of the 1.1 kpsi value appropriate for 144 inch lumber lengths to a value appropriate for the 59.5 inch "length" in our third point tests. See section 8.4.3 in ASTM D1990.) The plot also contains a line labeled "Olsson". The "Olsson" line is the $y = x - 4 \times s_{\text{Olsson}}$ line where the s_{Olsson} value is two-thirds of our s value and reflects Olsson *et al.*'s 6.30 Mpa s estimate.

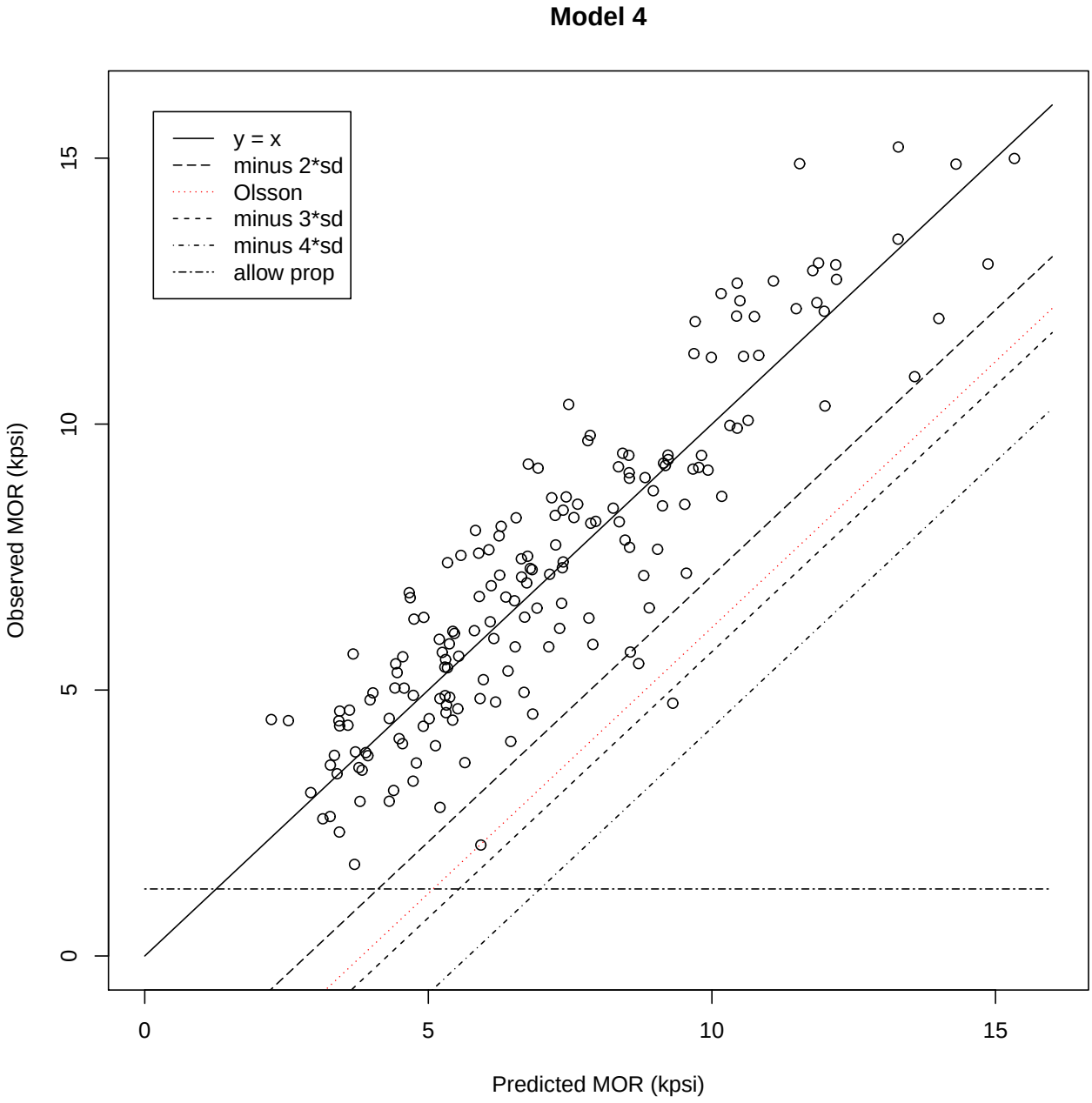

Figure 8: Plot of Model 4 observed versus predicted MORs together with $y = x$, $y = x - 2 \times s$, $y = x - 3 \times s$, $y = x - 4 \times s$, and $y = 1.26$ lines. Only **No. 2 data** is plotted. (Here we use 1.26 kpsi as the allowable property value for No. 2 Southern Pine 2x4 lumber. This corresponds to an adjustment of the 1.1 kpsi value appropriate for 144 inch lumber lengths to a value appropriate for the 59.5 inch "length" in our third point tests. See section 8.4.3 in ASTM D1990.) The plot also contains a line labeled "Olsson". The "Olsson" line is the $y = x - 4 \times s_{\text{Olsson}}$ line where the s_{Olsson} value is two-thirds of our s value and reflects Olsson *et al.*'s 6.30 Mpa s estimate.

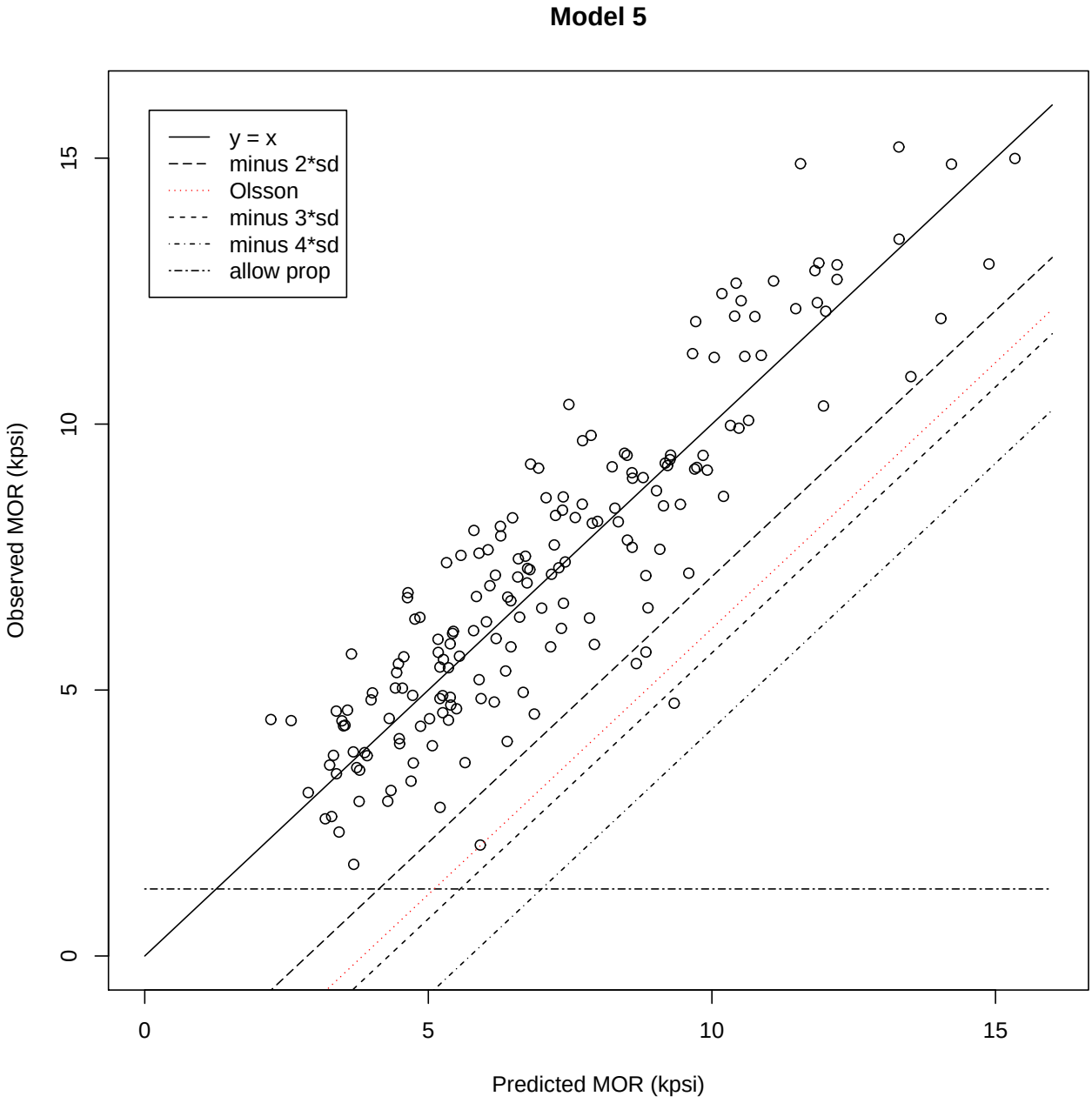

Figure 9: Plot of Model 5 observed versus predicted MORs together with $y = x$, $y = x - 2 \times s$, $y = x - 3 \times s$, $y = x - 4 \times s$, and $y = 1.26$ lines. Only **No. 2 data** is plotted. (Here we use 1.26 kpsi as the allowable property value for No. 2 Southern Pine 2x4 lumber. This corresponds to an adjustment of the 1.1 kpsi value appropriate for 144 inch lumber lengths to a value appropriate for the 59.5 inch "length" in our third point tests. See section 8.4.3 in ASTM D1990.) The plot also contains a line labeled "Olsson". The "Olsson" line is the $y = x - 4 \times s_{\text{Olsson}}$ line where the s_{Olsson} value is two-thirds of our s value and reflects Olsson *et al.*'s 6.30 Mpa s estimate.

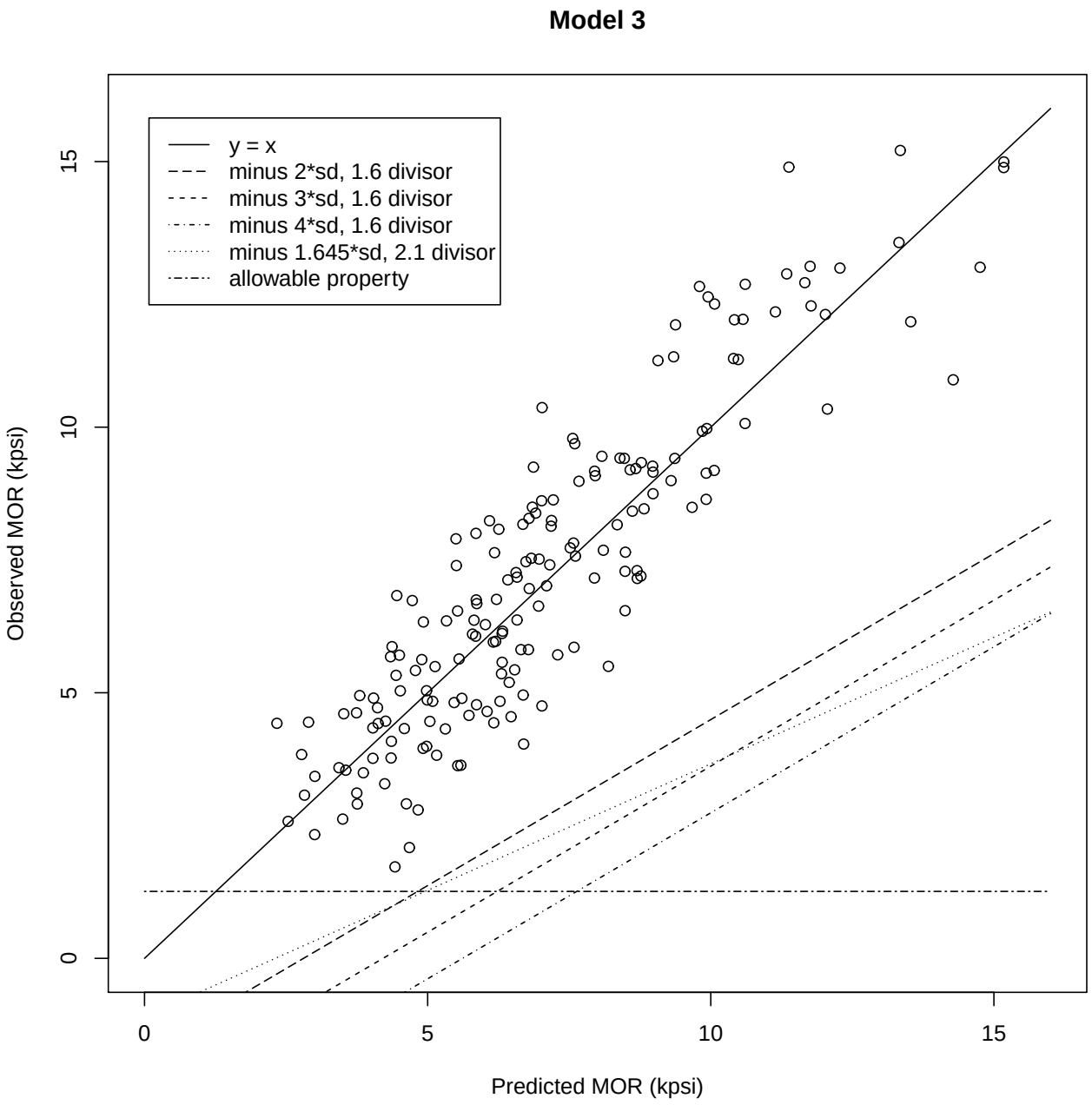

Figure 10: Plot of Model 3 observed versus predicted MORs together with $y = x$, $y = (x-2\times s)/1.6$, $y = (x-3\times s)/1.6$, $y = (x - 4 \times s)/1.6$, $y = (x - 1.645 \times s)/2.1$, and $y = 1.26$ lines. Only **No. 2 data** is plotted. (Here we use 1.26 kpsi as the allowable property value for No. 2 Southern Pine 2x4 lumber. This corresponds to an adjustment of the 1.1 kpsi value appropriate for 144 inch lumber lengths to a value appropriate for the 59.5 inch "length" in our third point tests. See section 8.4.3 in ASTM D1990.)

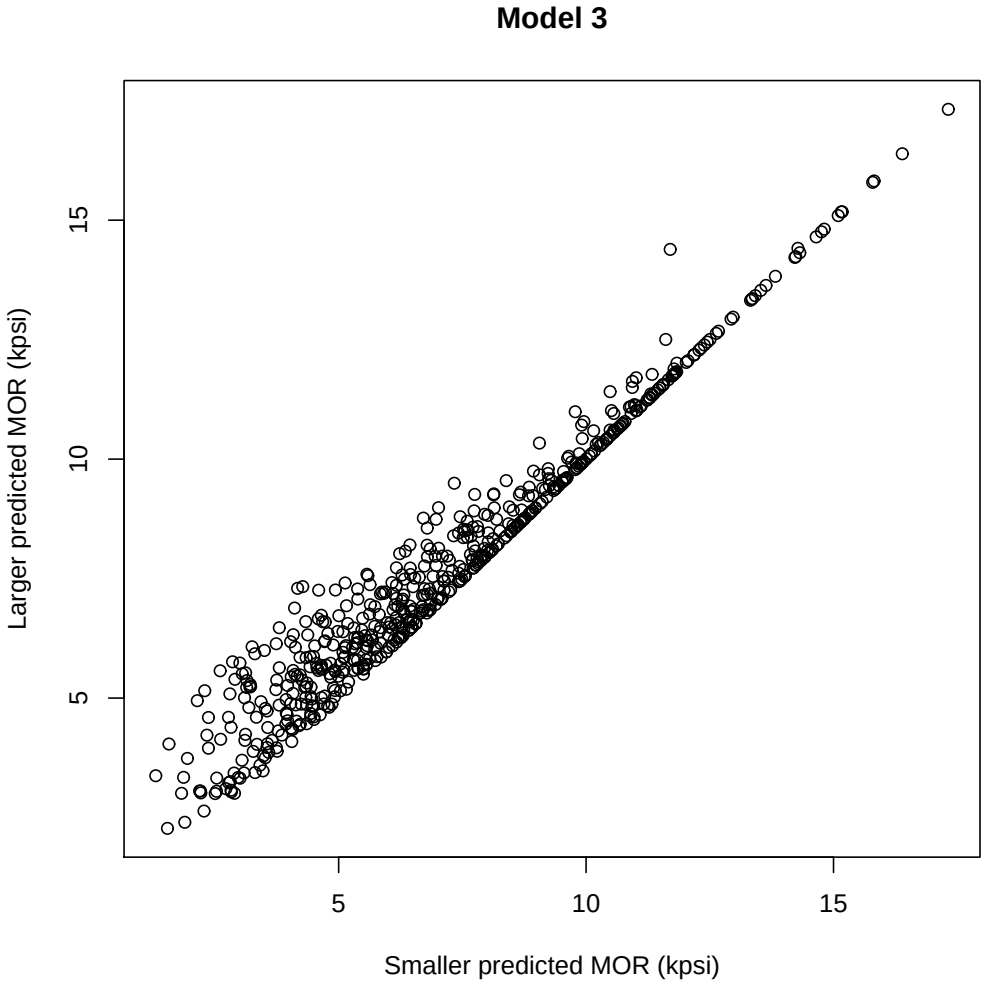

Figure 11: "Flipping a board" (exchanging compression and tension edges). Plot of larger predicted strength versus smaller predicted strength. Model 3.

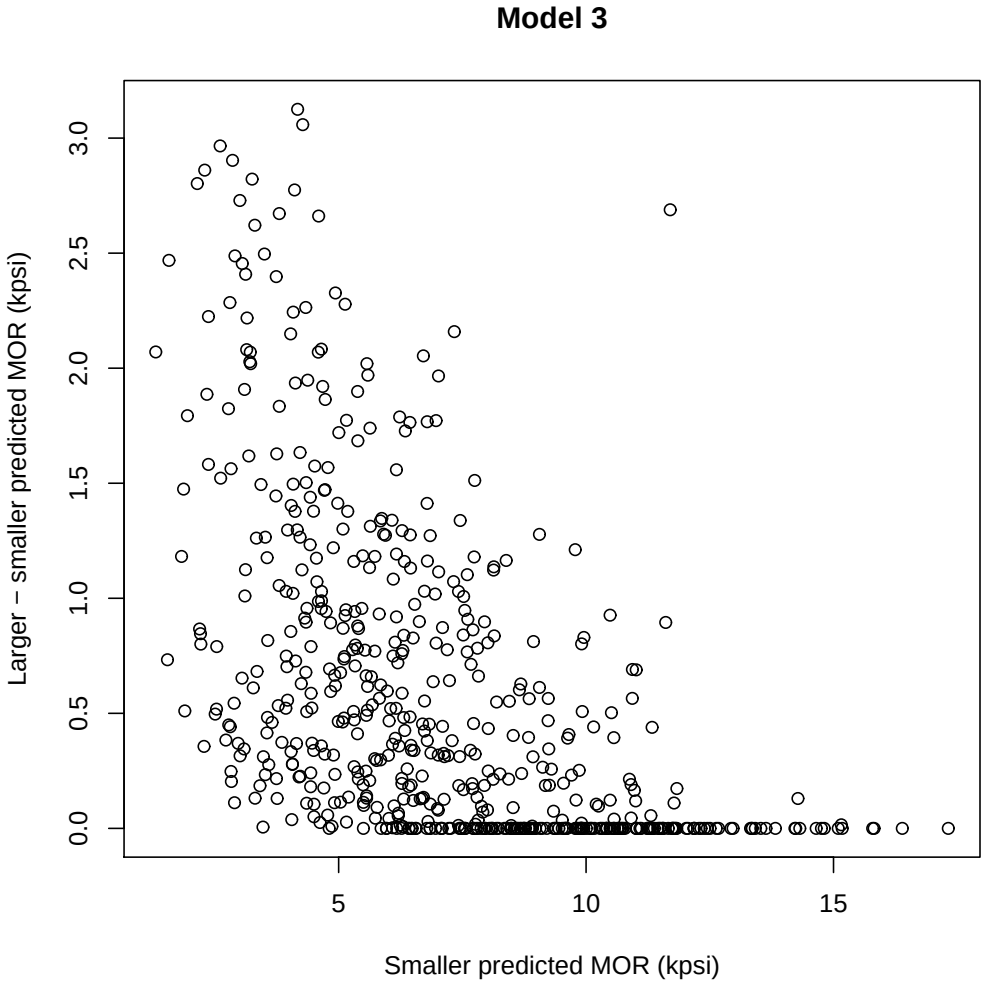

Figure 12: "Flipping a board" (exchanging compression and tension edges). Plot of larger minus (same board) smaller predicted strengths versus the smaller predicted strengths. Model 3.

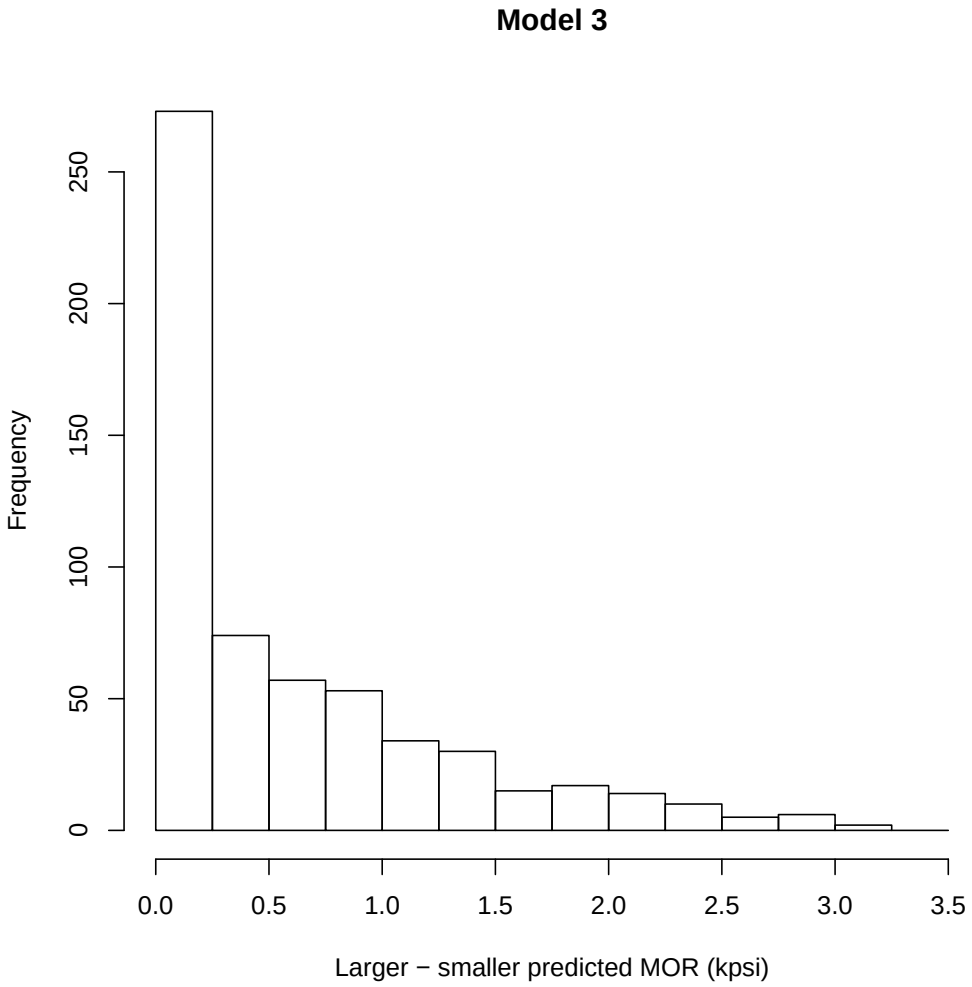

Figure 13: "Flipping a board" (exchanging compression and tension edges). Histogram of larger minus (same board) smaller predicted strengths. Model 3.

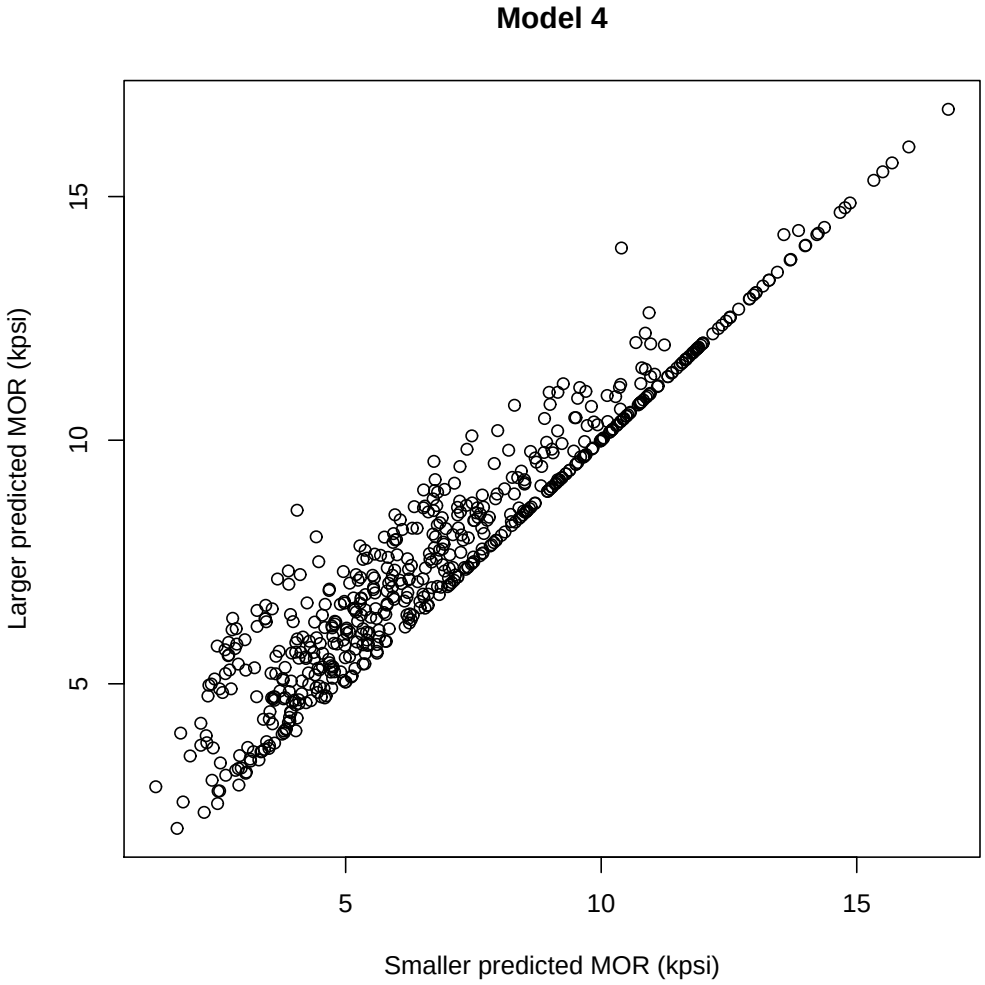

Figure 14: "Flipping a board" (exchanging compression and tension edges). Plot of larger predicted strength versus smaller predicted strength. Model 4.

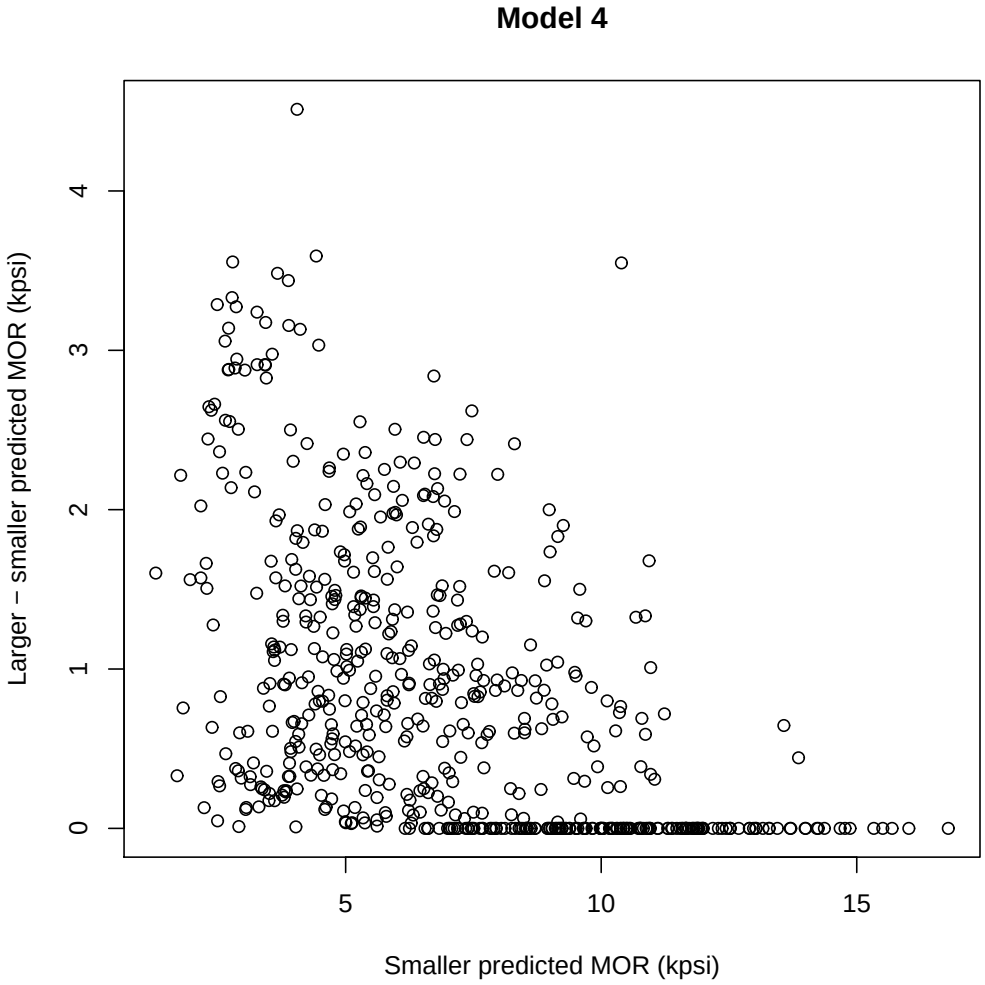

Figure 15: "Flipping a board" (exchanging compression and tension edges). Plot of larger minus (same board) smaller predicted strengths versus the smaller predicted strengths. Model 4.

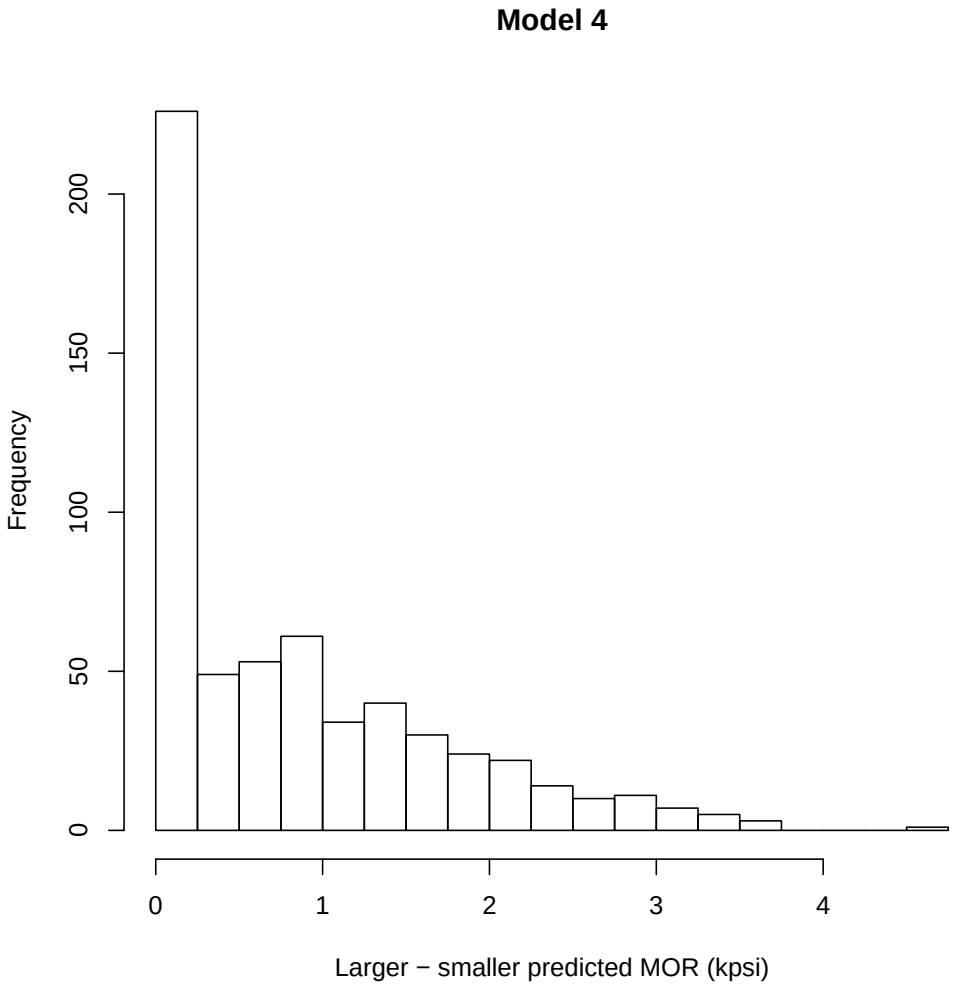

Figure 16: "Flipping a board" (exchanging compression and tension edges). Histogram of larger minus (same board) smaller predicted strengths. Model 4.